# "Computational Study of Magnetic Behaviour in Ni-Adsorbed Nb₂C MXene using Density Functional Theory"



## Zarah Khan

## Regn. 321161

A thesis submitted in partial fulfilment of the requirements

for the degree of **Master of Science**

in

**Physics**

**Supervised by: Dr. Syed Rizwan Hussain**

Department of Physics

School of Natural Sciences

National University of Sciences and Technology

H-12, Islamabad, Pakistan

2021

# National University of Sciences & Technology

## MS THESIS WORK

We hereby recommend that the dissertation prepared under our supervision by: ZARAH KHAN, Regn No. 00000321161 Titled: **"Computational Study of Magnetic Behavior in Ni-Adsorbed Nb2C MXene using Density Functional Theory"** accepted in partial fulfillment of the requirements for the award of **MS** degree.

### Examination Committee Members

1. Name: DR. ZEESHAN ALI                    Signature:

2. Name: DR. FAHEEM AMIN                    Signature:

External Examiner: DR. SIKANDAR AZAM        Signature:

Supervisor's Name: DR. SYED RIZWAN HUSSAIN    Signature:

Co-Supervisor's Name: DR. MUDASSIR IQBAL    Signature:

_____
Head of Department

4/8/2021.
_____
Date

## COUNTERSINGED

Date: 04/08/2021

**Dean/Principal**

# Declaration

I certify that this research work titled *Computational Study of Magnetic Behaviour in Ni-Adsorbed Nb$_2$C MXene using Density Functional Theory* is my own work. The work has not been presented elsewhere for assessment. The material that has been used from other sources it has been properly acknowledged / referred.

Signature of Student

Zarah Khan

2019-NUST-MS-Phy00000321161

# Copyright statement

# Acknowledgements

This thesis becomes a reality with the kind support and help of many individuals. I would like to extend my sincere thanks to all of them

First and foremost, all praises to ALLAH ALMIGHTY for HIS showers of blessing and guidance throughout this thesis work to bring it to end successfully. It was only possible due to wisdom HE bestowed upon me, the strength, the peace of mind and good health to finish this work.

I would like to express my gratitude towards my beloved parents who had always be a constant support in this work. I am extremely grateful to them for their love, prayers, caring and sacrifices for educating and preparing me for the future.

I am extremely grateful to my supervisor **Dr. Syed Rizwan** whose insight and knowledge into the subject matter steered me through this research. Without his help and cooperation completing this degree would not have been an easy task.

I am grateful to the principal of the School of Natural Sciences **Dr. Rashid Farooq** and Head of the Department of Physics **Dr. Shahid Iqbal**, for their suggestions and support throughout this program.

I am also very thankful to **Dr. Saleem Ayaz Khan** for his guidance in theoretical calculations and continuous guidance in understanding the Wien2k software.

Besides, my most sincere gratitude to **Jameela Fatheema** for giving good advice and being therein all the tough times.

And my biggest thanks to my husband **Armaghan** for all the support he had shown me through this research. It was his support that keep me going through the way.

I do believe that Allah Almighty has put me into field of science for many reasons and it is the part of my life to find and discover them.

*I, dedicate this thesis and my entire educational career to my father Aziz Ullah Khan, my mother Farah Naheed Aziz, who taught me to trust and believe in Allah and Islam, and especially for all the love, care, and prayers they have given me are boundless. They are the reason of my success and source of fulfilling my dreams.*

*My special dedication to my Brother Salman Khan and my Sister Fatima Khan, for their continuous support and always being there.*

# Abstract

2-dimensional metal carbides are freshly known as promising members, due to their encouraging applications. Among all the properties of MXene, their magnetic nature is researched vaguely in both experimental and theoretical fields. This property needs to be explored for the probable use in new upcoming applications such as spintronics and nano magnetic data storage devices. In the last 30 years, the quantum mechanical simulation of the cyclic systems has been done using density functional theory. Recently, it is widely used for the simulation of different structures and studying their electronic, optical, and magnetic properties. This thesis presents an insight to the magnetic properties of functionalized $Nb_2C$ MXene and its adsorbed compound Ni-$Nb_2C$ using Density Functional Theory. The $Nb_2C$-O-F and Ni-$Nb_2C$-O-F are simulated using DFT implemented software Wien2k. A unit cell of $Nb_2C$-O-F is simulated consisting of 4 atoms of Nb, 2 Carbon, 3 Oxygen atoms and 1 Fluorine atom. This unit cell simulated was further expanded in $2 \times 2 \times 1$ supercell and optimized at about 500 k-points in the irreducible Brillouin zone. Similarly, $4 \times 4 \times 1$ supercell is used to analyse the stable structure for Ni absorbed $Nb_2C$-O-F. The analysis for the magnetic properties in done using exchange-correlational functionals spin-GGA and spin-GGA+U where for Nickel U= 6 eV. The band structure for both compounds is found to be metallic with zero band gap. The magnetic moment calculate for $Nb_2C$-O-F is -0.00027 $\mu_\beta$. Although the value is small but confirms it diamagnetic behaviour and superconductive nature. The magnetic moment calculated for Ni-$Nb_2C$-O-F is +1.01516 $\mu_\beta$ which shows that it is non-superconducting Ferromagnet. This switching of magnetic behaviour clearly shows that the adsorbent along with surface terminations had influenced the magnetic property of $Nb_2C$-O-F.

## Table of Contents

# List of Figures

# List of Abbreviations

| | |
|---|---|
| **GMR** | Giant magnetoresistance effect |
| **DFT** | Density Functional Theory |
| **HF** | Hartree Fock |
| **KS** | Kohn-Sham |
| **H-K** | Hohenberg Kohn |
| **HEG** | Homogenous Electron Gas |
| **GGA** | Generalized Gradient Approximation |
| **MGGA** | Meta Generalized Gradient Approximation |
| **LDA** | Local Density Approximation |
| **LSDA** | Local Spin Density Approximation |
| **SCF** | Self Consistent Field |
| **RMT** | Radius Muffin Tin |
| **APW** | Augmented Plane Wave |
| **APW+LO** | Augmented Plane Wave + local orbitals |
| **LAPW+LO** | Linear Augmented Plane Wave + local orbitals |
| **LAPW** | Linear Augmented Plane Wave |
| **FP-LAPW** | Full Potential - Linear Augmented Plane Wave |
| **XRD** | X-Ray Diffraction |
| **FM** | Ferromagnetic |
| **GUI** | Graphical user interface |
| **DOS** | Density of states |
| **TDOS** | Total Density of States |

# List of Tables

# Chapter 01

# Introduction

Nanoscience discoveries and nanotechnologies have made life easier in this era in almost all fields of sciences. This nanotechnology and nanoscience represent a wider exploration field, that includes structures, devices, and systems with unique characteristics and operations due to the composition of their atoms on the 1–100 nm scale.[1] Nanomaterials are the main structures that are designed and produced by nanotechnologies with any one dimension at the size level of approximately less than 100 nanometres. Nano materials are structured intentionally with precise characteristics related to figure, size, and surface because the behavioural properties of nanomaterials are influenced more by surface area than particle structure itself. Based on dimensions restricted at nano scale, nano materials are classified as 1 dimensional, 2 dimensional and 3 dimensional. [2]
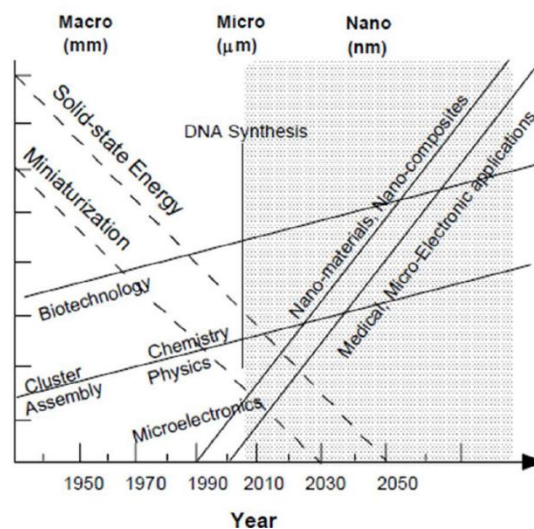


**Fig.1.1** Advancements in Science & Technology and the Future

2D materials are an emerging family of nanostructured small-dimensional materials having a thickness of a few nanometres or less. With the passage of time since the invention of graphene there has been other 2D materials that had attracted the attention researchers. These materials include transition metal dichalcogenides, hexagonal-boron nitride, MXene and 2D perovskite. Among all these 2D materials, MXene are of great interest. In 2011, Gogotsi et al. presented a study in which they have etched MXene from MAX, here "M" represents a

transition metal, "A" is group an element of periodic table, "X" is C or N [3]. The recent research on MXene includes both, theoretical and experimental discoveries but still there is a lot to be discovered and researched about this material as still some of its properties are not explained.

As much as the magnetism in 2D MXene is analysed, it stays less researched, and this lag needs to be covered soon. In this thesis the analysis is done based on density functional theory. The structure is synthesized by computer simulation and its magnetic and electric properties are observed while employing density functional theory DFT using the software package Wein2k.

## 1.1    Spintronics

From the time since giant magnetoresistance effect (GMR) are discovered and implemented in today's era, spintronics has become a striking field, intending to make advantage of electrons spin degree of freedom as an information exporter to accomplish data storage and logical operations. [4,5,6]

Spintronic devices need small amount of energy to switch over a spin state in comparison to conventional microelectronic devices that work because of charge. These spintronic devices work faster with lesser energy utilization. Hence, spintronics is the greatest advance technology to create different multi-functional devices with fast-speed and less energy consumption.

2D nanomaterials are considered of great capability for the development of later production 2D spintronic applications. [7,8,9] Just as graphene shows high-level electron or hole flexibility, long spin lifetimes and diffusion lengths, that make it to a likely applicant for a spin channel. [10,11] Different physical phenomena are observed in 2D materials that lead to magnetism and super conductivity. Superconductivity and magnetism in two-dimensional (2D) materials are intriguing phenomenon that can make advancements in spintronics devices.

With this as a motivation for study, 2D transition metal carbide MXene and its doped compound is synthesized. The magnetism and superconductivity are observed in both materials. Since the experimental procedures come with lot of issues, hence the DFT technique is used for analysis of electronic and magnetic properties.

## 1.2    Thesis Organization

The organization of this thesis is briefed to give a detailed information about its arrangement and the outlines. The first chapter explains the research topic briefly along with its motivation for studying.

The second chapter is related to literature review. It gives an insight of 2D materials; especially explaining MXene: a newly introduced family of metal carbides, nitrides or carbonitrides. Furthermore, different properties and applications of MXene are discussed continued with focusing on its magnetic behaviour. Magnetism in 2D nano materials is great area of research as it can be used for different applications such as superconductivity, 2D magnets and in field of spintronics. This thesis mainly focusses on the magnetic characteristics of MXene. Magnetism is discussed in detail in literature review. The properties that are the reason for magnetism are also discussed. Different methods such as absorbance, intercalation and doping that are used to alter the properties of MXene are also discussed. MXene and its literature work-based on Density functional theory using computational techniques is also explained in the chapter.

Chapter three consist of the experimental part. It explains about the procedure for the selective etching of Nb2C MXene and the procedure for its doping with Nickel. The research tools used for characterization are also explained in this chapter. The characterization technique used is X-Ray Diffraction (XRD) for examining the structure of prepared compounds.

Fourth chapter introduces density functional theory (DFT) in detail in the simplest way which is used for the theoretical simulations of MXene and finding its magnetic behaviour along with other characteristics. For explaining DFT, the discussion starts from Schrodinger wave equation (SWE) which is followed by the Hohenberg Kohen theorems and then ends with the Kohn-Sham equation which is used for the simulation purposes in WIEN2k. Moreover, the different plane-wave methods are briefed in detail and the basis for the choice of Full-Potential Linear Augmented Plane Wave (FLAPW) method are also discussed as well.

Chapter five is related to the detailed discussion of the results calculated for the two prepared compounds. The first part explains the experimental results of materials and the second part explains the computational results. For MXene and its doped compound, the computational analysis has been studied through electronic structure, band structure and DOS calculations as well as the magnetic moment.

In last chapter i.e., chapter 6, the thesis conclusion is given along with recommendations for future computation.

# CHAPTER 02

## Literature Review

## 2.1        Nano structured materials

Nanomaterials are widely regarded as the foundation of nanotechnology and nanoscience. Nanostructure science and knowledge is extensive and multidisciplinary field of study and invention that has grown in popularity in recent years. This study field has produced advances in materials synthesis, product development, and the variety and kind of functions accessible. It already has a significant business influence, which will undoubtedly grow in the future.

Nanomaterials are described as objects with at least one dimension that is smaller than 100 nm. A nanometre is 100,000X tiny than the thickness of a human hair and is one millionth of a millimetre. Because of their unique magnetic, optical, electrical, and various characteristics, nanomaterials are of interest. These changing characteristics have significant implications in a variety of applications such as electronics, medicine, and other disciplines. [12]
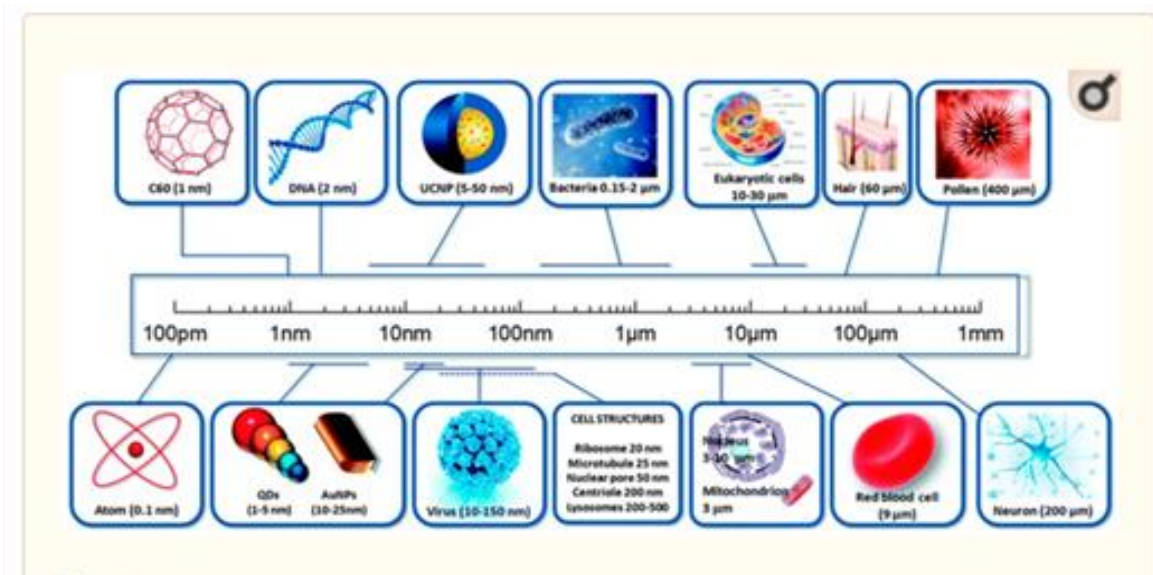


**Fig 2.1**   Different sizes of nanomaterials. Reproduced with permission from reference [13]

Nanoscale materials exhibit unusual emergent characteristics for two reasons: first, they have increased relative surface area, and second, they have novel quantum results. Nanomaterials

consists of considerably higher surface area to volume ratio than traditional materials that can reduce the strength and increase its chemical response. Furthermore, quantum effects at the nanoscale have the potential to become considerably more prominent in influencing the characteristics of materials, leads to new electrical, optical, and magnetic capabilities. [14]

Nanomaterials are very tiny, with at least one dimension of 100 nano meters or less. These materials are categorised as 0D, 1D, 2D, or 3D. (See Figure 1.3.) 1D structures have two dimensions ranging from 1nm to 100 nm, with a third dimension at the macroscale. Similarly, 2D structures have a single dimension ranging from 1nm to 100 nm. In the case of 0D, all three dimensions are in the nanometre range.

Nanowires, Nano belts, nanotubes, and surface films are examples of one-dimensional nanomaterials; Nano sheets, Nano plates, strands or threads are examples of two-dimensional nanomaterials; and particles are examples of three-dimensional nanomaterials. These nanomaterials can exist as fused, single, aggregated, or agglomerated structures with tubular, spherical, or non-linear geometries. Dendrimers, nanotubes, and quantum dots are examples of common nanomaterials. Different uses of these structured nanomaterials in the discipline of nanotechnology exhibits chemical and physical properties that differ in comparison to regular chemicals.

Among these nanostructured materials, 2 Dimensional materials are now gaining attention in the scientific community. Since the discovery of graphene and its extraordinary characteristics, 2D materials have become a significant parameter in material science study. We will address the computational study of 2D MXene with an emphasis on its magnetic characteristics in this thesis. Nickel metal is dopped in 2D metal carbide MXene and computationally analysed for in-depth examination. Furthermore, the characteristics of both metal carbide and doped material are thoroughly examined.
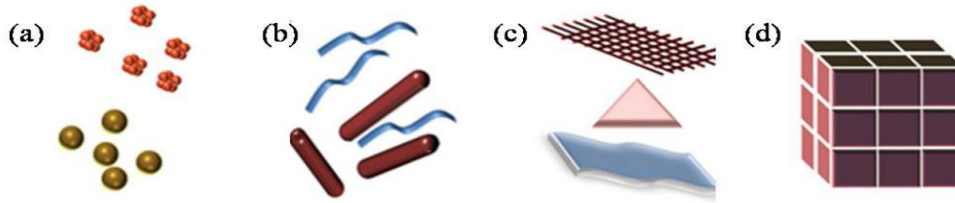
**Fig 2.2** Nanomaterials Classification (a) Sphere and cluster of 0D; (b) 1D nanofiber and nano-rods; (c) 2-D nanofilms nano plate nanosheets; (d) 3-D nanomaterial

# 2.2 MXene; 2D Metal Carbides, Carbonitrides or Nitrides

MXene is a modern family of two-dimensional material derived from transitional metal carbide, carbon nitride and nitride. Gogotsi et al. proposed these 2-D transitional metal carbide, carbon nitride and nitride (MXenes) [15] in 2011, which has lately sparked renewed interest in the evaluation of advanced ideas and their prospective applications in the area.

MAX phases consist of three-layered metal carbides, nitrides, or carbon nitrides precursors having the generalised formula: $M_{n+1} A X_n$ (n = 1, 2, 3), where d-block transition metals are represented by M and A represents carbon. These are s-p elements (mostly from group IIIA or IVA), and X in formula represents both C and N atoms. This stacked precursor is used to create the layered 2D nanostructure known as MXene. These novel materials are created via a selective chemical etching technique. As shown in Fig. 2, the layer of s-p elements is particularly etched from the appropriate three-dimensional MAX precursor. Surface terminations such as -F, -O, and -OH are adsorbed on plane surface of MXene throughout the chemical etching process. These terminated MXene (space group P63/mmc) exist characterised by the generic formula $M_{n+1} X_n T_x$, here M represent Transition Metal, T is the plane surface termination, and x is the percentage of such surface terminations. Till date, further 70 MAX phases have been published [16], and the successfully synthesized MXene are more than thirty which include $Ti_3C_2T_x$ , $Ti_2CT_x$ , $Mo_2TiC_2T_x$  and $Nb_4C_3T_x$ . [17,18]
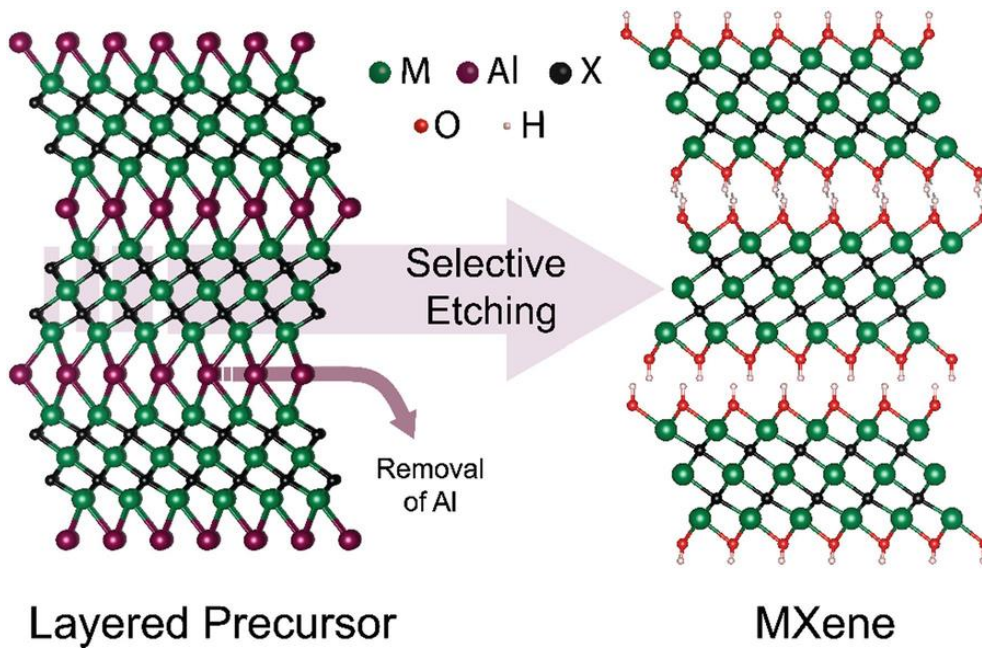
**Fig 2.3** MAX phase precursor and MXene structure
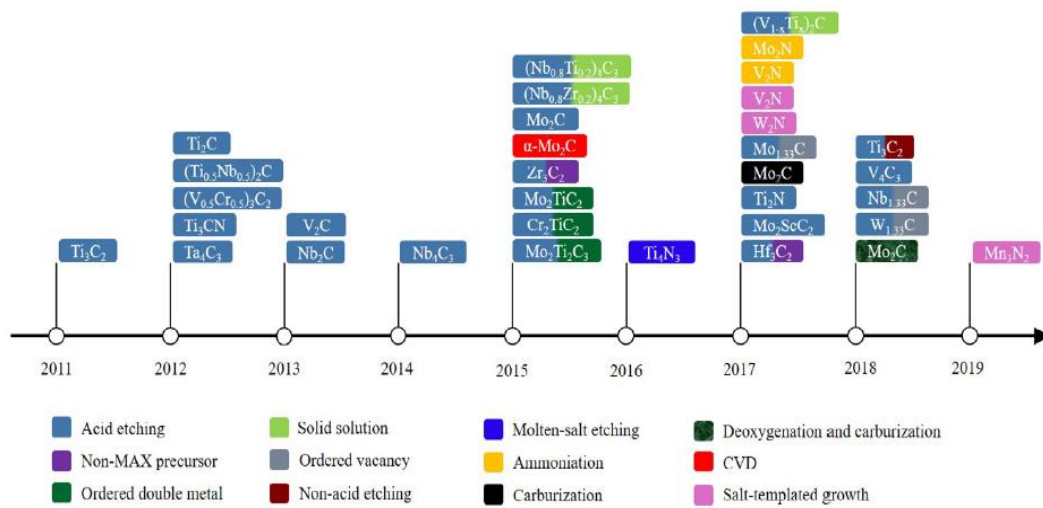


**Fig 2.4** Time of MXene; 2D nanomaterial

Many studies have been published since the discovery of MXene that give evidence for its remarkable properties. MXene conductivity, for example, is shown to be like that of multi-layered graphene. [19]

MXene is shown to be very stiff by density functional theory (DFT) analysis, with in plane elastic constants surpassing 500 GPa.[20] Such intriguing characteristics have resulted in significant applications and have aroused the interest of academics in a variety of disciplines.

## 2.2.1    Applications of MXene

The distinctive morphology of the MXene makes it a solid contestant for applications that have a very important role in the daily life technologies. Several of those applications and the studies related are mentioned below.

- MXene shows some extremely productive electrode matter for energy conversion devices for example triboelectric nanogenerators [21] and water splitting devices. [22]
- It's also been reported for energy storage application like super-capacitors and batteries, along with other applications including capacitive purification and electromagnetic interference defending. [23] MXene are promising electrode materials for energy storage. [24]

   • Xie et al. investigated MXene as support material of platinum nanoparticles, resulting in extremely stabilized catalyst of fuel-cell applications. [25]

   •Wang et al. discovered 2D MXene had good enzyme immobilisation abilities as well as biocompatibility for redox proteins, indicating that they have potential uses in electrochemical biosensors. [26]

Comparing the opto-electro-magnetic characteristics and its subsequent applications received less attention.[27] Furthermore, there has been a rise in the number of innovative applications of MXene and opto-electro-magnetic phenomena in this field of study. Superconductivity [28], 100 percent spin purity half-metallic behaviour [29], and high Curie temperature ferromagnetism [30] are a few examples. Aside from that, recent developments in MXene and related composites are being employed in the construction of gadgets such as Li-based batteries, such as $Li^+$-ion batteries and Li–sulphur batteries.

## 2.2.2    Structural Characteristics and Properties of MXene

MXene has a tightly filled structure with X and M atoms saturating the octahedral interstitial spaces. MXene has an overall hexagonal tightly packed crystal structure. The arrangement of M atoms, however, swapping as of $M_2X$ to $M_3X_2$ and $M_4X_3$. M atoms in $M_2X$ have ABABAB

arrangement, i.e., hexagonally tightly packed pile up, whereas M atoms in $M_3C_2$ and $M_4C_3$ have ABCABC arrangement, i.e., FCC pile up. [31] as demonstrated in figure below:
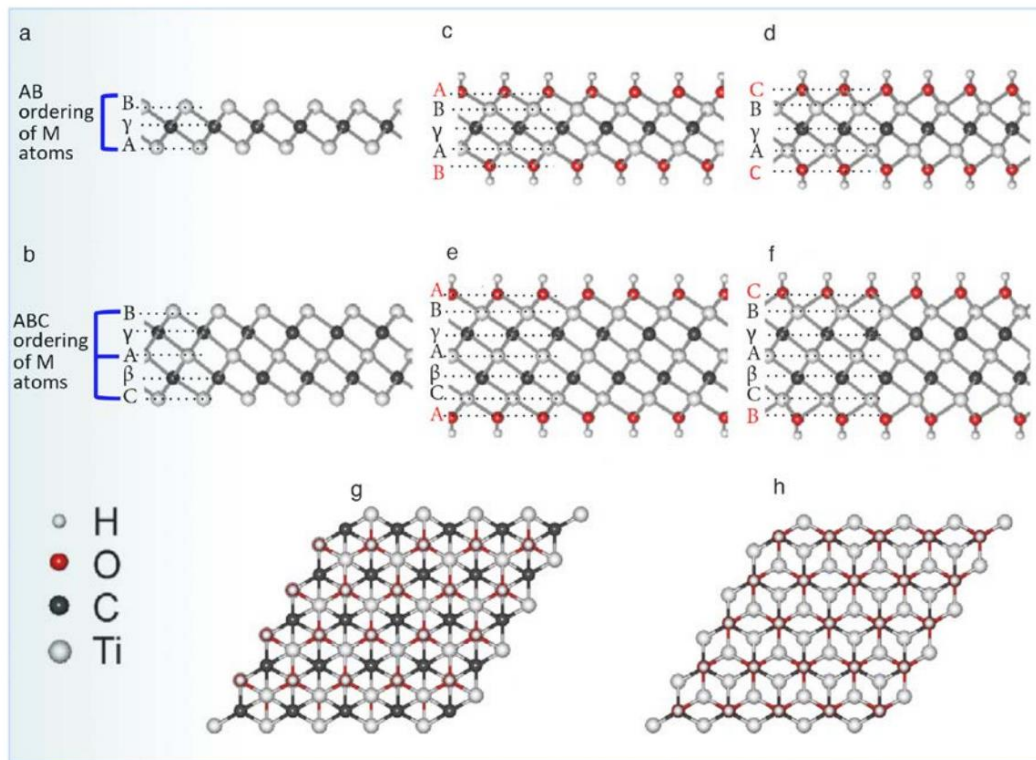


**Fig 2.5** MXene Crystal atomic arrangement of M, X and T elements

The optimised arrangement of (a) separate $Ti_2C$ layers and (b) $Ti_3C_2$ layers are given above, and their hydroxylated forms are presented in (c) and (d), i.e., $Ti_2C(OH)_2$, and (e, f) is $Ti_3C_2(OH)_2$. (c, e, g) depict OH groups are placed in the empty location among their three neighbouring carbon atoms. The OH groups are present at top of the carbon atom, as displayed in (g, h) in top view. The capital Greek and Roman letters relate to the X and M locations in this case. Greek letters in lowercase indicates the interstitial sites of X octahedral, which represents their Roman letter equivalent locations, namely, A, B, and C, respectively. [31]

## 2.2.3        Surface terminations

MAX phases have a crystalline structure characterised as a pile up of transition metal carbide octahedrons incorporated with a plane of unmixed A atoms. [32] The A layers of MAX crystal formations are removed during the selective etching technique. As a result of the revealed M-site atoms' higher reducibility, MXene is reactive to the solvent and etchants. When reaction take place and Metal atoms releases an electron, negative charged groups in the surrounding establish connections with the Metal atoms to guarantee charge preservation, resulting in

terminations. As a result, MXene plane takes in surface terminations like O, F, and OH. [33] Especially MXene made through acidic-HF- solutions have a combination of –OH, –O and –F surface terminations. These are commonly represented as $M_{n+1}X_nT_x$, where surface termination is represented by T.

They frequently have exceptional electrical, mechanical, optical, thermal, and catalytic characteristics. [34] According to studies, the physical characteristics of MXene, such as the band [35], metallicity, electronic mobility, and magnetism, are strongly related to the end points. [34] Furthermore, by altering the surface terminations of MXene, the electrochemical performance may be adjusted.

Several experimental experiments have shown that the surface composition of freshly produced MXene varies significantly. [36] However, experimental characterisation of MXene surfaces is difficult due to

(i)     lighter components such as H, O, and F are contained by the surface.
(ii)    After etching process, the contaminated surface, and remaining precursors
(iii)   Alteration in the experimental circumstances provoke systematic studies.


As a result, computational investigations are preferred for comprehending these surface terminations. Surface terminations in supplement to the characteristics of bare $M_{n+1}X_n$ layers, have recently been computationally investigated [31]. Many researches have been linked with single functional groups just as pure –OH, –F or–O and described the characteristics of MXene using surface terminations. [31]
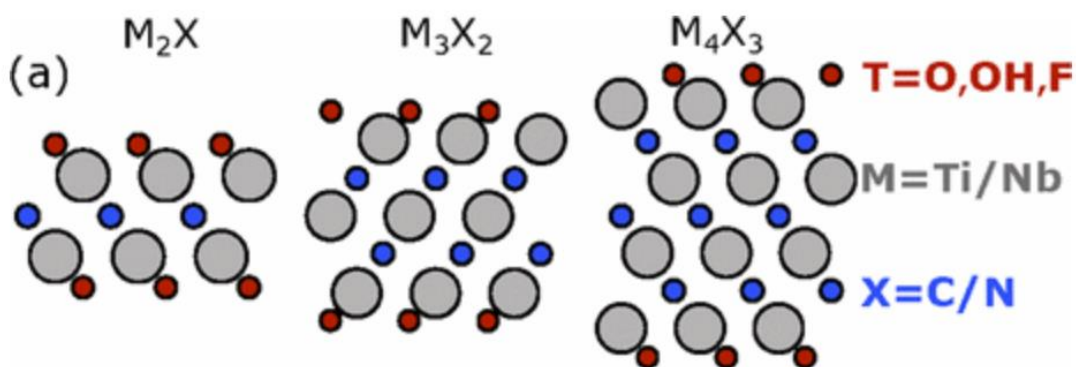


**Fig 2.6**  Lateral-view of the MXene of various thickness: $M_2X$, $M_3X_2$ and $M_4X_3$ [33]
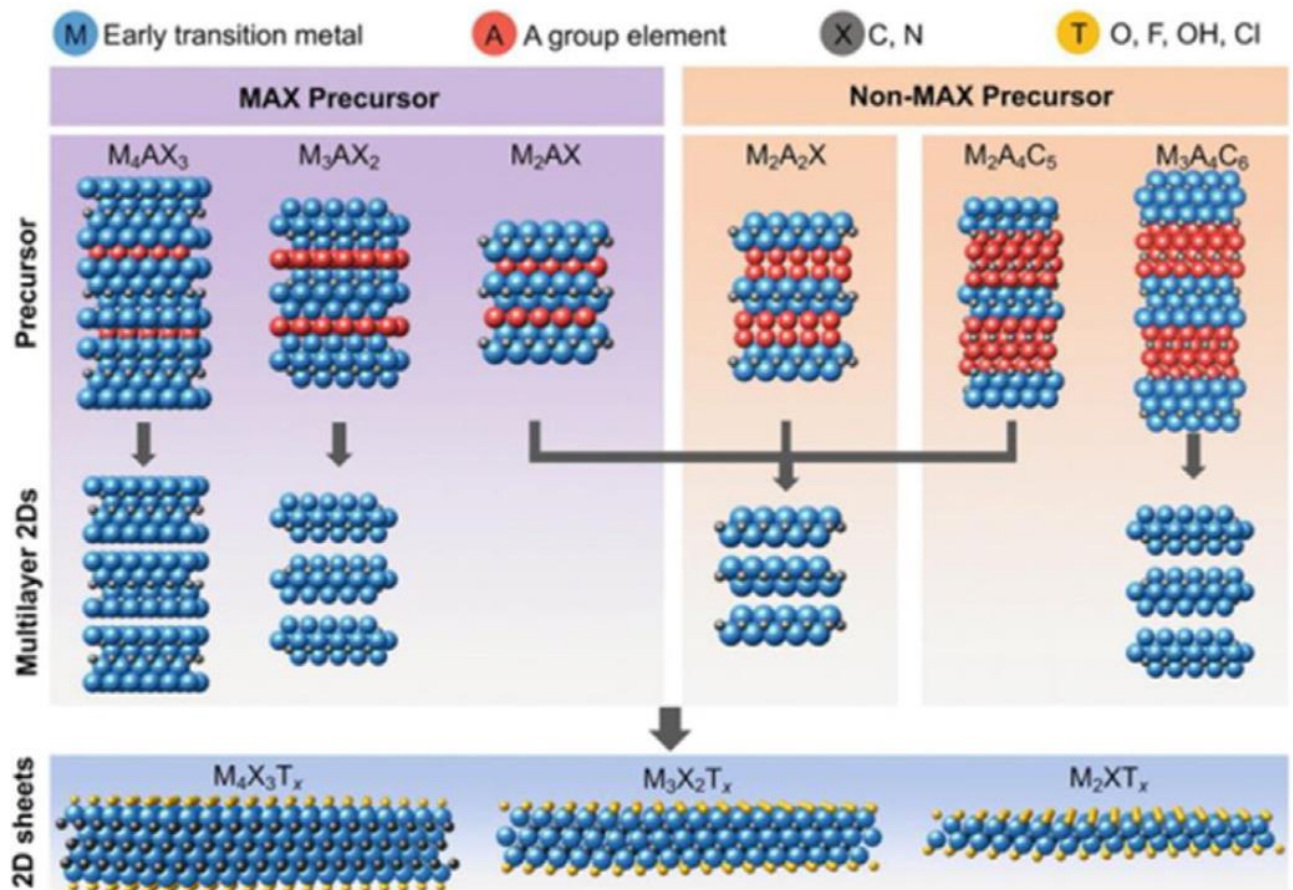
**Fig 2.7** Major types of MXene $M_2XTx$, $M_3X_2Tx$ and $M_4X_3Tx$ [37] and its synthesis

The kinds of terminations resulting from the various techniques are recorded in table below. Pros and Cons of each strategy are summarized [32]

| Strategies | Terminations | Advantages | Disadvantages |
|---|---|---|---|
| HF-based etching | –F, –OH, –O, –Cl | ■ High efficiency<br>■ Universal | ■ Toxic<br>■ Eco-unfriendly |
| Molten salt etching | –Cl, –Br or –I | ■ Nearly single termination | ■ High-temperature synthesis (> 600 °C) |
| Alkali-based etching | –OH, –O | ■ Non-toxic | ■ Low efficiency<br>■ High-temperature, high-pressure synthesis |
| Electrochemically assisted etching | –Cl, –O | ■ Non-toxic | ■ Low efficiency<br>■ Over-etching |

**Table.1**　　　Types of Surface terminations resulting from synthesis techniques

Various MXene investigations have been conducted depending on the influence of surface terminations. T. Schultz et al. uses density functional theory calculations, inverse photoelectron spectroscopy and photoelectron spectroscopy to analyse the electronic characteristics of $Ti_3C_2T_x$ for distinct surface terminations resulting from various annealing temperatures. The adsorption locations of the surface terminations were determined by comparing experimental and DFT simulations. [38] MXene is a significant material for energy storage applications because of its surface terminations. MXene has been described as a Charge Storage Host by M. Okubo et al. [39]

## 2.2.4　　　Intercalation

The capacity of layered materials to accept different subatomic particles among its sheets is called as intercalation. Intercalation is opposite to the insertion of molecules or ions into layered material formations when the structural properties of the host are not affected, just as graphite

and transition metal dichalcogenides. The perturbation of the geometric, chemical, electrical, and optical characteristics of the host materials by intercalated ions/molecules is what makes intercalation so intriguing for research. External species intercalation in 2D layered materials, such as MXene, differs significantly from intercalation in bulk materials, which results to improved characteristics for a variety of applications.[41] It has been discovered that the intercalation of external species, such as ions and solvents, into MXene layers during electrochemical processes has a significant impact on the energy storage process, prompting substantial research into its underlying processes and aiding the process. The intercalation phenomena are primarily employed in energy storage applications. The electrochemical intercalation of Li ions among the MXene sheets provide these solids materials for LIB anodes and Fusion Electrochemical capacitors Kajiyama et al. has reported sodium intercalation in $Ti_3C_2T_x$. He discovered that $Ti_3C_2T_x$ reaches 270 mAh/g at earliest sodiation process, while the lithium capability dropped to 100 mAh/g around 100 cycles.[43]

## 2.2.5 Defects, vacancies, and doping

The desire for portable contemporary electronic gadgets has increased the need to investigate the magnetism of electronic materials. Because 2D materials are new now, they have been an important part in experimental and theoretical research. However, the majority of 2D materials are nonmagnetic. The current study focuses on inducing and controlling magnetism in 2D non-magnetic materials. Since the produced materials usually have flaws just as microscopic disorder, hole, and contamination. These flaws have considerable influence on the electrical structure, magnetic and optical characteristics of 2D materials. Similarly, the as-prepared exfoliated MXene consist of native defects, such as atomic vacancies or etc.

**Defects** are studied comprehensively in 2D material just graphene, BN, and $MoS_2$. It has been demonstrated that electronic, electrical, and optoelectronic characteristics are greatly influenced. The defects result during the chemical etching process. Their intensity can be regulated by modifying the HF intensity. In case of milder etching conditions, larger MXene flakes are produced with lower defect concentrations.

X.Sang et al. has reported in his article the thorough knowledge of the monolayer structure and point defects. In the article, STEM tomography is operated on $Ti_3C_2T_x$ MXene with different off-tilt angles which showed existence of various point defects in $Ti_3C_2T_x$ monolayers. These point deficiencies influenced conductivity and surface composition which were investigated using DFT. DFT analysis suggested outstanding conductivity for the

compound which was further verified by direct experimental results deduced for exfoliated $Ti_3C_2T_x$ applications. [44]

The impact of imperfections on the electronic structure, formation energy, and magnetism of $Ti_2XT_2$ (where X is C/N and T can be OH-, F-, or O-) was investigated. The findings indicated that tiny amounts of point defect may instigate significant change in the magnetic and electrical characteristics of the $Ti_2XT_2$ material. A. Bandyopadhyay et al. found Schottky and Frenkel type defects in $Ti_2CO_2$ that cause band-gap fluctuation and assure metal-semiconductor transition. Schottky defect generation raises $Ti_2CO_2$'s narrower bandgap to 0.48 eV ($TiO_2$ defect) and 0.33 eV (TiC defect), whereas Frenkel type defect causes $Ti_2CO$ to shift from semiconductor to metal. [45]

Zhou et al. has presented a Ti or N hole defect that was studied for the surface layer of the $Ti_4N_3$ nanosheet. Furthermore, a frenkel-type defect is reported sandwiched between the N atom on the subsurface layer and the Ti atom on the top layer. The structural alteration, electronic characteristics, and magnetism of atoms in the vicinity of the defect atom were computed and analysed. [46]

**Doping** is done to initiate external element into 2D materials so that desirable properties can be achieved in the target material. Doping can cause different changes in material as it increases c-lattice parameter. The introduction of such imperfections and contaminations is beneficial for energy storage devices. Impurities in materials cannot be avoided during the chemical process and can be the reason in changing the properties of material.

J. Fatheema et al. worked on doped MXene and had reported Nb doped MXene synthesis and characterization. The computational and experimental analysis had shown Nb substituted MXene a ferromagnetic compound with improved chemical stability as compared to pure MXene due to successful doping and being a useful member in spintronic devices.[47]

S. Rafique et al. describes the productive doping of gadolinium to the MXene sheets. The doped MXene gives partial-conductive nature with decrease of the bandgap and initiation of strong ferromagnetic nature at room-temperature which makes it an appropriate applicant for spintronic applications. [48] M. Fatima et al**.** described the unique behaviour of the Nb-doped MXene bandgap, that gives an appropriate result for energy storage applications just as supercapacitors and Li-ion batteries. [49]

## 2.2.6 Magnetism in MXene

Although a significant amount of research is made on the electronic and optical characteristics of MXene but the magnetic properties of MXene for spintronics application are still unknown. Magnetism in MXene is an interesting subject for research. The native properties of MXene are defined by the transition metal M in the MAX phase precursor due to which most of the research associated to the magnetism of MAX phases was performed on V, Cr, Mn, and Mo based ternary carbides. [50] The MAX phases are found to be Pauli paramagnets i.e.; the magnetic sensitivity is defined by the delocalized electrons.

MXene family two-dimensional layers display a wide range of magnetic characteristics. MXene includes transition metals with unbound valence electrons, as well as transition metals whose valency varies with bond formation. Different forms of ferromagnetism and anti-ferromagnetism have been researched and anticipated in MXene, which alter with the M element as well as the phase of MXene.

The magnetic nature of MXene can result from:

i. self-properties of the transition metal,
ii. imperfections in mono layers
iii. surface terminations.
iv. synthetic procedures

Many theoretical investigations concern the magnetic $M_2CT_x$ structures based on V, Cr, Mn, Mo, and Fe, and their solid solutions. [51] 2D $Cr_2C$, $Cr_2N$, $Ta_3C_2$, and $Cr_3C_2$ are expected as ferromagnets [52,53] that can be obtained from their MAX phases, whereas 2D $Ti_3C_2$ and $Ti_3N_2$ are antiferromagnets. $Ti_2C$ and $Ti_2N$ have been shown to have almost half-metallic ferromagnetism [54]. Ferrimagnetic half-metals with total (100%) spin polarisation of electrons near the fermi level are interesting spintronic possibilities. MXene may be converted to ferromagnets by appropriate surface functionalization, which has been found and researched.

Although some pure MXene are expected as ferromagnets but experimental studies confirm that MXene are normally functionalized with F, O, OH or other atoms [55] since it is difficult to produce pristine MXene.

It is discovered that functionalized $Cr_2C$ and $Cr_2N$ MXene show magnetism [56,] but few of them demonstrate ferromagnetic-to-antiferromagnetic transitions. Hence this suggest that functionalized are not necessarily to be ferromagnets. Recently, Yoon et al. explored the

magnetic behaviour of $Ti_3C_2T_x$ reduced by Li-ethylenediamine and manifested that their powders to be Pauli paramagnets above 10K with a temperature dependent Curie term below this. [57] Scheibe et al. showed that etching Al from a $Ti_3AlC_2$ MAX phase resulted in $Ti_3C_2T_x$ MXene with a mixed antiferromagnetic/paramagnetic behaviour that depended upon the surface functionalization. [58]

## 2.3 Density Functional Theory (DFT) study of MXene

As already discussed above, nowadays 2D materials having TMC's have become a topic of considerable studies due to their unique properties that vary from the bulk phases. Computational attempts are used to cover the large class of 2D materials and enlarging field of their probable implementation. Obviously, theoretic approach is needed to study the properties of MXene, its structural details and to discover more elements of this family at a basic level.

 The recent advancement in theoretic study of MXene based on the computational results is explained in this section. Through DFT, structural, electronic, and magnetic properties of MXene had been studied by taking the generalized gradient approximation. The PBE exchange–correlational functional [59] is widely used means to study details of structures.

 Gogotsi et al. in 2011 exfoliated and etched MAX to obtains MXene first time successfully, along with presenting a DFT study of the crystal structure of $Ti_3C_2$ with its functional groups. Lattice parameters of MAX and MXene structure had also been discussed as well as an analysis on elastic properties. [60] Khazei et al. had reported the geometric and electronic properties of different layered MXene with their surface's terminations F, O, and OH groups. The article has described mechanical and thermodynamic stable surface terminated MXene systems. Without surface terminations, all the MXene are found metallic. DFT was used as a research tool to observe all properties of desired compound.[61] Khazei et al in another article related to 2D MXene has analysed the molybdenum carbides thermoelectric properties by taking density functional theory as research tool. [62] Hu et al. has reported their inquiries on $Nb_2C$ single-layer as a competitive anode for Lithium and Non-Lithium-ion Batteries based on DFT calculations. The electronic properties and the storage capabilities of the $Nb_2C$ monolayer and its subsequent fluoride and hydroxide materials were analysed in this article based on DFT. [63] For the first time, R. Momeni Feili has calculated the energy loss near edge structure (ELNES) of 2D MXene. Results are calculated by density functional theory using FLAPW method. The paper describes the ELNES spectra pattern of Nitrogen and Carbon K-edges for MAX $M_2AlX$

phases, pristine $M_2X$ and for functionalized $M_2XT_2$ (M = Sc; X = C/N; T = F, OH, O) at different angle conditions. [64] Meng et al. has reported S-functionalized $Ti_3C_2$ MXene material in his manuscript. For investigating various properties along with dynamic stability, DFT calculations were completed. The sodium storage ability of $Ti_3C_2$, $Ti_3C_2O_2$ and $Ti_3C_2S_2$ systems found were useful to design for anode material. [65] Chen et al. work describes $Ti_3CN$ MXene as an anode of a Li-ion battery. The process of Lithium-ion adsorption and dispersion on the surface of $Ti_3CN$ and $Ti_3CNT_2$ (T is F, O, and OH surface terminations) was analysed to evaluate the probable usage of $Ti_3CN$ as an anode material using DFT. [66] Li et al has reported the analysis related to the contacts sandwiched among lithium polysulfides (LiPSs) and $Ti_2CO_2$ substrate as well as other six $M_3C_2O_2$ MXene using DFT calculation. It had been proved in article, all six $M_3C_2O_2$ MXene systems acquired confining capacity towards soluble LiPSs.[67] Zbik et al. has reported the theoretical examinations of geometry and electronic structure of molybdenum carbide by DFT. The thermodynamic sensitivities obtained using DFT showed preparation of $MoO_3$ reduction to produce (oxo)carbides is Endo energetic. [68] Radzwan et al. reported different attributes of Ni doped $Sb_2S_3$ using FP-LAPW method-based DFT. The lattice parameters at equilibrium are analysed using PBE-GGA exchange correlational functional. The results calculated show that Ni-doped $Sb_2S_3$ has higher optical absorption coefficient than the pure-$Sb_2S_3$ which can be applied for optoelectronic devices. [69] Iqbal et al. have reported un-doped and Lanthanum-doped $Ti_3C_2T_x$ MXene, prepared by co-precipitation technique. The experimental results are obtained by DFT calculations. The magnetic characteristics for both compounds have been examined, demonstrating the existence of ferromagnetic-antiferromagnetic phases. [70] Babar et al. has stated the diamagnetic behaviour of successfully synthesized 2D-$Nb_2C$ and observance of superconductivity in the material. DFT calculation were achieved by DFT software using spin-GGA approximation. The magnetic moment is computed negative, which verifies accurately with the experimental results. [71] Fatheema et al. has reported experimental and computational magnetic phase calculations that indicates the switching from superconductive-diamagnetic behaviour to ferromagnetism in La-doped $Nb_2C$-O-F MXene. The computational analysis of pure $Nb_2C$ MXene verifies diamagnetism and moreover clearly explains the role of Lanthanum and surface terminations (O and F) in the decline of diamagnetism in La-doped $Nb_2C$-O-F while stimulating ferromagnetic behaviour.[72]

## 2.4        $Nb_2C$ (metal carbide) MXene

Many MXene have been synthesized and studied that includes $Ti_2C$, $Ti_3C_2$, $Ti_3CN$, $(Ti0.5Nb0.5)_2C$, $Ta_4C_3$, $Nb_2C$ and $V_2C$. [73] Among all of these, titanium carbide MXene are explored extensively to acquire awareness about the exceptional material implementation. Niobium carbide ($Nb_2C$) is minimum researched because of its extra ordinary significance in energy storage devices. Regardless of its unique magnetism and some useful physicochemical characteristics, most of the feasible implementations of niobium carbide are still to be discovered.

$Nb_2C$ MXene was first synthesized and reported by Naguib et al. and just described it as favourable electrode for the electrochemical activities. Further, different studies have reported $Nb_2C$ with various implementations such as biomedical applications, energy storage, supercapacitors, and nanoelectronics. [74]

Among different MXene, $Nb_2C$ is an encouraging applicant as an electrode in Lithium-ion batteries having higher capability and ability to handle high-level charge–discharge cycles.[75] Furthermore, $Nb_2CT_x$ have also shown favourable performances for photothermal cell ablation as well as a photo-catalyst for hydrogen progression. [76,77]

Regardless of the improvement in production, description and theoretical explanation, structural study on microscopic scale of MXene is very rare. STEM has previously been effectively applied for microscopic investigation of MXene. [78-80]

$Nb_2CT_x$ MXene sheets are prepared by removal of Al from $Nb_2AlC$. [81] In MXene the M-C (here M means Nb) have combined metallic- ionic-covalent bond which is stronger in nature compared to that of M-Al, weak metallic bond. [82.] Because of this behaviour, in presence of high temperature and hydrofluoric acid (HF), the M-Al bond is substituted by weaker hydrogen bond which results in the splitting of the sheets.

### 2.4.1       Structural Analysis

The XRD spectrum of $Nb_2AlC$ and synthesized $Nb_2C$ MXene is demonstrated in Fig. 2.8. The XRD pattern verifies hexagonal MAX Phase structure with space group $P6_3/mmc$. Selective removal of Aluminium from $Nb_2AlC$ shows the fading of peaks at 25.75°, 38.8°, 42.7°, 52.2°, 57.9° and the development of different peaks which indicates the transformation of the MAX into MXene. The decrement of peak 002 at an angle 12.79° and its shifting towards smaller angle 7.2°, indicate the structural change in structure. This shift and change give an improved

c-lattice parameter changing from 13.83 Å to 22.7 Å. The improvement in lattice factor is the reason for the increased interlayer spacing.
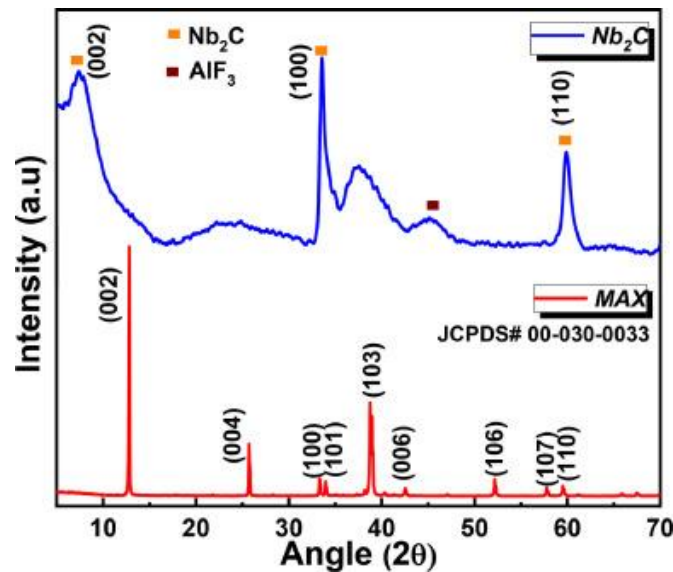


**Fig 2.8** XRD pattern for $Nb_2C$ and MAX $Nb_2AlC$. Fig reported by the permission of author [82]

SEM images of the structural morphology showed layered MXene traditional morphology. [83] The magnetic behaviour of MXene has been a less researched, with little report accessible on its magnetic behaviour. Their magnetic behaviour is found to be based on the transition elements which includes Cr, Mn, V, Fe, and Ni or in any doped conformations. Babar et al. mentioned about the magnetic behaviour of $Nb_2C$. The diamagnetic behaviour was observed in $Nb_2C$ MXene along with the Meissner effect, which showed superconductive nature in the material with transition temperature of 12.5 K [84]

## 2.4.2    DFT Study of $Nb_2C$ MXene

$Nb_2C$ MXene was designed in WIEN2k package, using the FLAPW approach. The structure was optimized and minimized, with 500 k-points used in the IBZ, with a k-mesh of 14 x 14 x 2 points.

Computational study confirms the diamagnetic magnetic behaviour of $Nb_2C$ MXene. $Nb_2C$ DFT was performed through Wein2K applying spin -GGA approximation. The value of magnetic moment calculated is – 0.00485, which means its diamagnetic. Hence above-mentioned computational study verifies the experimental results of $Nb_2C$ MXene. [84]

DFT is an effective and influential approach for estimating the electronic densities of state (DOS) as well as work functions of simulated materials. The quantum capacitance and electrostatic potentials of $Nb_2C$ MXene are also being calculated using ab initio DFT. has

reported in their article about a series of $Nb_2C$ MXene investigated and verified as possible electrode for super-capacitors and electron emission devices utilizing ab initio DFT computations. [85] All calculations were performed by exchange correlational functional PBE-GGA implemented in CASTEP package. The plane-wave energy cut-off was set to 540 eV and k-mesh of $12 \times 12 \times 1$ used in irreducible Brillioun zone (IBZ).

Quantum capacitance of bare $Nb_2C$ MXene is found to be five times more than that of graphene and bare $Nb_2C$ MXene is found to be the best candidate among all Niobium Carbides $Nb_{n+1}C_n$ MXene owning the greatest quantum capacitance at both positive and negative electrodes. [85]

It is also known that few-layer $Nb_2C$ MXene can be used for photoelectrochemical-type photodetectors (PDs). $Nb_2C$ nanosheets exhibit a great capability for small-band photodetectors. Gao et. Al has reported and verified this by calculating work functions predicted by density functional theory calculations. Hence these fascinating outcomes reveal $Nb_2C$ nanosheets can be utilized as basics units for different photoelectronic applications, beyond expanding the application possibilities of 2D MXene. [86]

# Chapter 03

# Experimental Techniques and Research Tools

## 3.1  Experimentation

Two compounds were prepared experimentally. 2D $Nb_2C$ MXene sheets were prepared from 3D MAX Phase precursor (i.e., $Nb_2AlC$). After successful selective etching, $Nb_2C$ was doped with Nickel (Ni). Both the compounds synthesized were characterized through XRD, SEM and EDS

### 3.1.1  Selective Chemical Etching of $Nb_2AlC$

**Materials**

The materials used during the selective etching process are:

- Hydrofluoric (HF) acidic mixture (50 wt. % in $H_2O$, $\geq$99.99%)
- Niobium Aluminium Carbide Powder ($Nb_2AlC$, purity 97 % with 200 mesh)
- De-ionized water
- Ethanol

### 3.1.2  Procedure

i.  Two dimensional MXene was prepared from $Nb_2AlC$ MAX phase precursor through selective wet chemical etching method.

ii.  For successful etching results, 1 g of $Nb_2AlC$ MAX powder was immersed in 100 ml of HF (50% wt.) at ratio of 1:10 in Teflon beaker. The solution was constantly stirred for 40 hrs by Teflon-coated magnetic stirrer.

iii.  The temperature was optimized to be at 55 ℃. The resulting deposits were washed many times with deionized water through centrifugation process for 5 minutes at 3500 rpm until the pH of supernatants was achieved to be ~6. [87]

iv. The HF eliminates the Al layer, which, in sequence is replaced by F, O and/or OH. Every time, the supernatant was separated, and the powder settled at the bottom was removed from centrifuge bottles using ethanol.

v. The resulting MXene powder was dried in vacuum oven at 40℃ for 24 hrs.

vi. The resulting MXene was achieved in full amount without major losses.
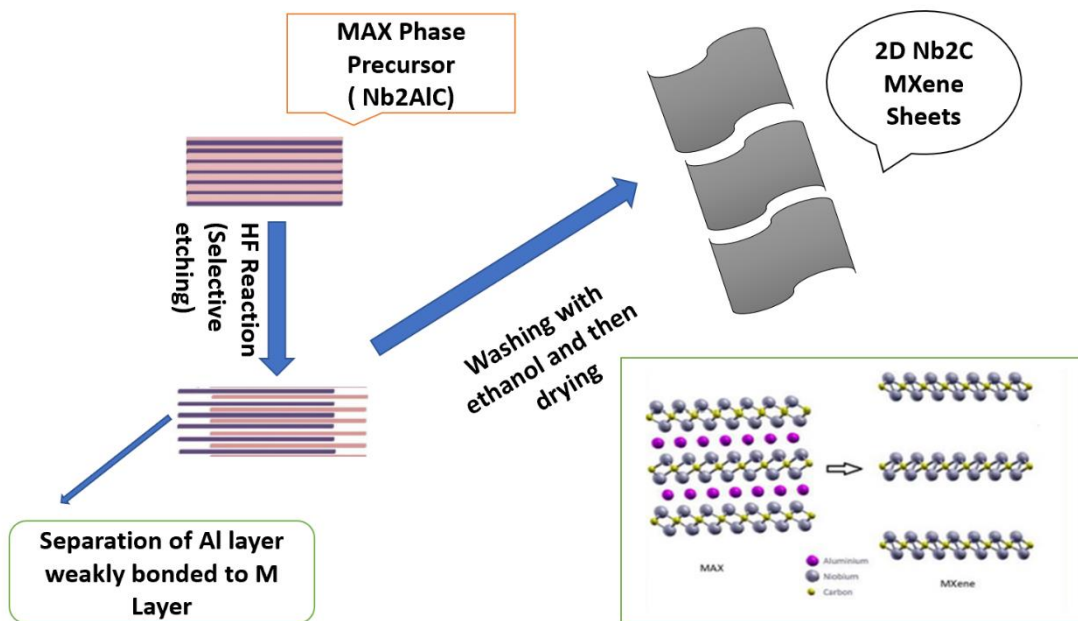


**Fig 3.1** Schematic diagram of $Nb_2C$ synthesize from $Nb_2AlC$ precursor

## 3.1.3    Nickel Doped Nb₂C MXene Preparation

i. Ni doped $Nb_2C$ MXene was prepared by a straightforward hydrothermal method [88]

ii. $Nb_2CT_x$ powder was mixed in 30 ml deionized water by magnetic stirring for half-hour.

iii. The precursor solution was made by dissolving the crystals of nickel nitrate hexa-hydrate Ni $(NO_3)_2.6H_2O$ in 20 ml deionized water.

iv. The two prepared solutions were mixed, then magnetically stirred for 20 minutes. During the magnetic stirring, 50 % ammonia was added until pH was achieved to be 9.

v.  The final solution was then shifted to a Teflon lined autoclave made of stainless steel (70 ml) at 90℃ for 16 hrs. Later, the reaction mixture was cooled at room temperature.

vi.  The resultant precipitates formed were washed by deionized water and dried in convection oven at 60℃ for 24 hrs.

vii.  The end dried product was stored in a glass vial and collected for further characterization.

# 3.2 Research Tool

For analysis of the prepared materials, the crystallographic, structural, and morphologic characterization is done using the research tool. X-Ray Diffraction (XRD). XRD of the dried powdered sample is completed by using Bruker D8 Advance system.

## 3.2.1 X-Ray Diffraction (XRD)

XRD is the most widely applied technique for the examination of crystal shapes and atomic spacing. XRD works on the phenomenon of constructive interference of monochrome X-rays and a crystal-clear sample. The crystalline nature of materials is examined by the XRD by measuring the diffraction of X-rays from the planes of atoms within the material.
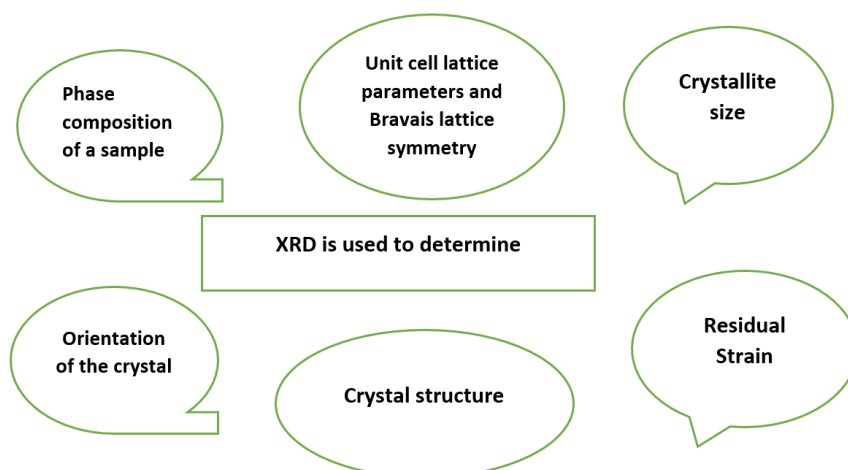


**Fig 3.2** Uses of XRD Analysis

The working principle of XRD is based on Bragg's Law, which was first introduced by Sir W.H. Bragg and his son Sir W.L. Bragg. This law explains when the incident x-ray strikes the crystal surface, at an incident angle, $\theta$, it reflects with a same scattered angle $\theta$. The path difference d, if found equal to a whole number n, and wavelength, a constructive interference takes place. Mathematically,

$$n\,\lambda = 2d\sin\theta$$

here $\lambda$ represents wavelength of the x-ray, d is the space between the crystal layers (i.e., path variation), $\theta$ is the angle of incidence, and n is an integer.
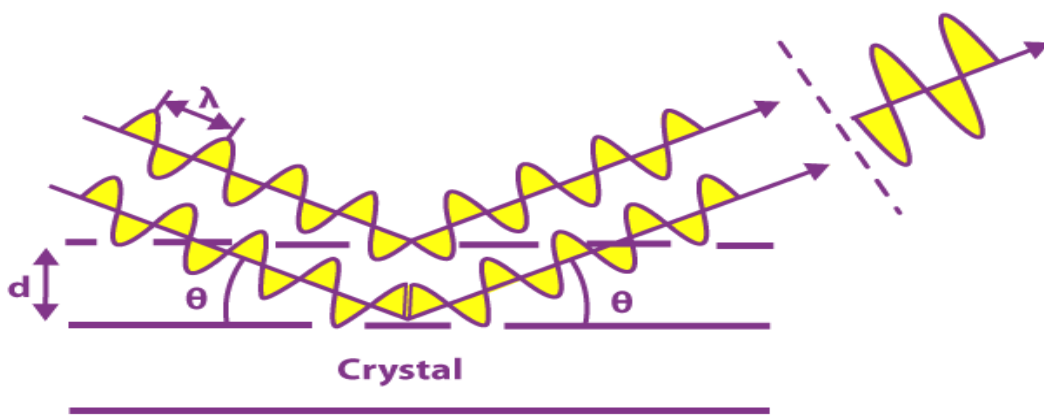
**Fig 3.3** Braggs Law

This law is related to the wavelength of x-rays and the space between the crystal layers in a crystal-clear sample. The diffracted X-rays from the sample are then spotted, managed, and calculated.

# Chapter 04

## Computational Techniques

Nowadays a lot of advancements have been made which have a substantial role in the study of material and in enhancing the efficiency of the materials for our use. Studying materials in detail by using computers has been cost effective for us. Therefore, computational are mostly used for studying material. The theoretical study that provides the basis of this computational study is condensed matter physics and density functional theory (DFT) and many other theories. The theoretical study can be performed without any prior knowledge of the system as well as when the system is known and to create an understanding for the experimental system that is at micro or nano level at the atomic level in angstroms.

This chapter concentrate on the density functional theory, its development, and a brief introduction of the usage through the software package WIEN2k.

## 4.1 Density Functional Theory (DFT)

Density functional theory is used as a research tool in this thesis. Currently DFT is one of the efficient and effective quantum mechanical method, to investigate different characteristics of matter. It is used as an approach to study the structural, electronic, magnetic, and optical characteristics of material at quantum level.

DFT considers the ground state charge density to measure the ground state attributes of a system. Here the ground state charge density is a functional which used the wave function of electron as an input. In solving a simple system just like hydrogen atom, Schrodinger wave equation (SWE) is used but with atoms in large amount in a system the number of variables and terms also increase. Hence it becomes difficult to solve such system by using SWE. This leads us to the need of an equation which will have to be easier to solve.

### 4.1.1 Schrodinger wave equation (SWE) and many bodies problem

In 1926, Erwin Schrodinger, derived an elaborate equation for a system using the de-Broglie's hypothesis, where the wave function contains the information of the whole system and Hamiltonian is described for the energy of the whole system. [89]

SWE for simple system just electron moving in potential field is given as:

$$\left[\frac{\hbar^2}{2m}\nabla^2 + V(r)\right]\Psi = E\,\Psi \qquad \ldots\ldots\ldots \quad 4.1$$

$$\hat{H}\,\Psi = E\,\Psi \qquad \ldots\ldots\ldots \quad 4.2$$

here
$$\hat{H} = \left[\frac{\hbar^2}{2m}\nabla^2 + V(r)\right] \qquad \ldots\ldots\ldots \quad 4.3$$

From above equation 4.3, we have

$$\hat{H} = \hat{T} + \hat{V} \qquad \ldots\ldots\ldots \quad 4.4$$

where
$$\hat{T} = \frac{\hbar^2}{2m}\nabla^2 \quad \text{and} \quad \hat{V} = V(r) \qquad \ldots\ldots\ldots \quad 4.5$$

$\hat{H}$ represents the Hamiltonian operator, $\hat{T}$ is kinetic energy and $\hat{V}$ is the potential. $\Psi$ gives wave function of an electron.

## 4.1.2     Born-Oppenheimer Approximation

A strong solid structure is defined as a body consisting of heavy positive particles (nucleus) and lighter negative particles (electron). When a simple system (as mentioned above) is modified or replaced by many atoms, such as if taking N nuclei, then the system is dealing with a problem of N+ZN interrelating particles. This system is called a quantum many-body problem. The numerous-particle Hamiltonian for this system is given as:

$$\hat{H} \quad = \quad -\sum_{I=1}^{N_n}\frac{\hbar^2}{2m}\nabla^2{}_{R_i} \quad - \quad \sum_{I=1}^{N_e}\frac{\hbar^2}{2m}\nabla^2{}_{r_i} \quad + \quad \frac{e^2}{4\pi\epsilon_0}\left[-\frac{1}{2}\sum_{I=1}^{N_n}\sum_{I=1}^{N_e}\frac{Z_I}{|r_i-R_I|} + \right.$$

$$\left.\frac{1}{2}\sum_{I=1}^{N_n}\sum_{J\neq I}^{N_n}\frac{Z_I Z_J}{|R_I-R_J|} + \frac{1}{2}\sum_{i=1}^{N_e}\sum_{j\neq i}^{N_n}\frac{1}{|r_i-r_j|}\right] \qquad \ldots\ldots\ldots\ldots \quad 4.6$$

The first two terms represent kinetic energy of nuclei and electrons in a system, respectively. While the remaining terms give the potential energy due to electron-nucleus interaction, nucleus-nucleus interaction, and electron-electron interaction, respectively. In equation M is the mass of a nucleus at $R_I$ while m is the representation of mass of electron at $r_i$. Since the nuclei are considerably heavy particles and far slower than the electrons. Hence, they are considered having fixed positions and the electrons are assumed to be in immediate equilibrium with them. This is called as **Born-Oppenheimer approximation**. It was introduced by Born-

Oppenheimer in 1927. [90]. After applying this approximation, we are only left with the negative charge particles. Hence due to no motion of nuclei, their kinetic energy is zero and therefore the first term vanishes. The last term is considered constant. The equation is reduced to form containing the kinetic energy, the potential energy for electron-electron interactions and the potential energy of the electrons in the potential of the nuclei. This statement is summarized as

$$\hat{H} = \hat{T} + \hat{V} + \hat{V}_{ext} + \hat{V}_{nn} \quad ………….\ 4.7$$

$$\hat{T}_e = \sum_{i=1}^{N_e} -\frac{1}{2}\nabla_{r_i}^2, \quad V_{ext} = -\frac{1}{2}\sum_{i=1}^{N_e}\sum_{I=1}^{N_n}\frac{Z_I}{|r_i - R_I|} \quad V_{nn} = \frac{1}{2}\sum_{I=1}^{N_n}\sum_{J\neq I}^{N_n}\frac{Z_I Z_J}{|R_I - R_J|}$$

$$V_{ee} = \frac{1}{2}\sum_{i=1}^{N_e}\sum_{j\neq i}^{N_e}\frac{1}{|r_i - r_j|}$$

After applying the Born Oppenheimer approximation, the system is modified but still it is challenging to solve such system. Different procedures are present to reduce this equation to a flexible form. One of these methods is the Hartree-Fock method (HF). This approach works perfectly for atoms and molecules and is used in quantum chemistry. For solid systems it is found less precise. However, in this thesis our focus is on Density Functional Theory.

In the year 1964–65, the basis of Density Functional Theory was placed by Hohenberg–Kohn during their first paper on DFT which described that any property of a system in ground state is a unique functional of the ground state electron density. [90]

## 4.1.3      Hohenberg-Kohn Theorems

DFT is basically based on two main theorems.

### Theorem I

The ground state energy from Schrodinger's equation is a unique functional of the electron density. Or in other words, there exists one-to-one correspondence between the ground-state density $\rho(\vec{r})$ of a many-electron system and between the potential $V_{ext}$. The ground-state expectation value of any observable $\hat{O}$ is defined as a unique functional of the exact ground-state electron density and is described as:

$$\langle\Psi|\,\hat{O}\,|\Psi\rangle = O\,[\rho] \qquad \ldots\ldots\ldots\ldots \text{4.8}$$

Before moving towards the proof of this theorem, the term functional is defined. If there exists a one-one correspondence between two quantities, then it is defined as a functional.

For the proof of this theorem three quantities are kept under consideration: Potential V(r), wave function $|\Psi\rangle$ and the electron density $\rho(r)$. A one-one mapping (Map D and Map E) should exists as follows:

$$\textbf{Map D} \qquad\qquad \textbf{Map E}$$

$$\text{V(r)} \longrightarrow \quad |\Psi\rangle \quad \longrightarrow \quad \rho(r)$$

$$\longleftarrow \qquad\qquad \longleftarrow$$

$$\textbf{Map D}^{\text{-1}} \qquad\qquad \textbf{Map E}^{\text{-1}}$$
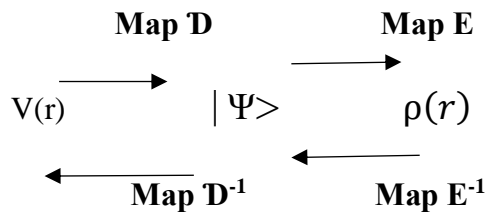
To prove it, considering the inverse mapping between the quantities. Consider

$$V' \neq V'' + \text{constant}$$

Since
$$\hat{H}\,\Psi = (= T + U + V')\,\Psi \qquad \ldots\ldots\ldots\ldots \text{4.9}$$

$$\hat{H}\,\Psi = E\,\Psi$$

Similarly,
$$\hat{H}'\,\Psi' = (T + U + V'')\,\Psi' \qquad \ldots\ldots\ldots\ldots \text{4.10}$$

$$\hat{H}'\,\Psi' = E'\,\Psi'$$

As $V' \neq V''$ so for the one-one correspondence, $\Psi$ and $\Psi'$ should be different.

Taking
$$\Psi = \Psi',$$

$$(V' - V'')\,\Psi = (E - E')\,\Psi'$$

$$(V' - V'') = (E - E')$$

Hence
$$\Psi \neq \Psi' \qquad \ldots\ldots\ldots\ldots \quad \text{4.11}$$

Thus, for every ground state wave function, there corresponds a potential value V(r) and this proves D$^{\text{-1}}$ mapping exists.

Now to prove the next inverse mapping, considering the variational principle. From variational principle

$$E = (\Psi| \hat{H} | \Psi) < (\Psi'| \hat{H} | \Psi') \quad \ldots\ldots\ldots\ldots \quad 4.12$$

The above equation represents the non-degeneracy of the system. Now,

$$(\Psi'| \hat{H} | \Psi') = (\Psi'| \hat{T} + \hat{U} + \hat{V}' | \Psi')$$

$$= (\Psi'| \hat{T} + \hat{U} + \hat{V}' + \hat{V} - \hat{V}' | \Psi')$$

$$= (\Psi'| \hat{H}' | \Psi') + (\Psi'| \hat{V} - \hat{V}' | \Psi')$$

$$= E' + \int \rho'(r) \, [v(r) - v'(r)]$$

From equation 4.12

$$E < E' + \int \rho'(r) \, [v(r) - v'(r)]$$

Similarly

$$E' = (\Psi'| \hat{H}' | \Psi') < (\Psi| \hat{H}' | \Psi)$$

$$E' < E + \int \rho(r) \, [v'(r) - v(r)]$$

Hence if $\rho(r) = \rho'(r)$ then $E + E' < E' + E$ which is not possible. This proves that $\rho(r) \neq \rho'(r)$ and there exists only one electron density for each wave function $\Psi$. Hence the 1st theorem is proved.

From the 1st theorem it was stated that ground state energy from Schrod. Equation is a unique functional of electron density. To find which electron density, we proof the 2nd theorem. [90]

**Theorem II**

The electron density that reduces the energy of the overall functional is the true electron density corresponding to the full solution of the Schrodinger equation. $\hat{O}$ taken as the Hamiltonian $\hat{H}$, the ground-state total energy functional $H[\rho] \equiv E\, V_{ext} [\rho]$ changes as:

$$E\, V_{ext} [\rho] = <\Psi| \hat{T} + \hat{V} | \Psi> + <\Psi| \hat{V}_{ext} | \Psi> \quad \ldots\ldots\ldots \quad 4.13$$

$$E\, V_{ext} [\rho] = F_{HK}[\rho] + \int \rho(\vec{r}) \, V_{ext} (\vec{r}) \, d\vec{r} \quad \ldots\ldots\ldots\ldots \quad 4.14$$

In above equation 4.14 Hohenberg-Kohn (HK) density functional $F_{HK}[\rho]$ is found comprehensive for any many-body electron system.

Taking $\qquad\qquad\qquad E \equiv E[\rho]$

Therefore, $\qquad\qquad E[\rho] = (\Psi[\rho]\vert \hat{H} \vert \Psi[\rho])$

For trail ground state density, $\overline{\overline{\rho}}\,(r)$

$$E \equiv E\,\overline{\overline{[\rho]}} = (\Psi^{\overline{\overline{}}}\overline{\overline{[\rho]}} \vert \hat{\overline{\overline{H}}} \vert \Psi^{\overline{\overline{}}}\,\overline{\overline{[\rho]}}\,)$$

From variational principle,

$$\overline{\overline{E}} > E \qquad \text{For } \rho \neq \overline{\overline{\rho}}$$

$$\overline{\overline{E}} = E \qquad \text{For } \rho = \rho^{\overline{\overline{}}}$$

The above two conditions clearly state the theorem and hence its proved.

Since electron density is functional of wave function therefore the above equation reduces to form

$$E[\{\Psi_i\}] = E_{\text{Known}}[\{\Psi_i\}] + E_{XC}[\{\Psi_i\}]$$

The term consists of Kinetic Energy, coulomb interactions between electron and nuclei, between electron pairs and between pairs of nuclei whereas the $2^{\text{nd}}$ term is called and **Exchange Correlational Functional**. It consists of all the quantum impacts not incorporated in known terms.

## 4.2 Kohn Sham Equations

Although, HK theorems present the electron density $\rho$ (r) as the basic variable, it is still unmanageable to find and evaluate properties of a system because the universal functional $F[\rho(r)]$ is not known. The Kohn and Sham equations were announced in 1965 that turn DFT into a practical tool to obtain the ground state density of the system. They mapped a system of interrelating electrons on to a system of non-interacting electrons that has the same ground state

density and ground state energy [90]. The electrons in this system are not interacting with each other but every electron feels the field generated by all the other electrons.

For non-interacting electrons

$$\left(-\frac{\hbar^2}{2m}\nabla^2 + v\right)\phi = E\,\phi \qquad \text{......... 4.15}$$

For large system, taking total energy E as

$$E = \sum \varepsilon i$$

For interacting electrons

$$\left(-\frac{\hbar^2}{2m}\nabla^2 + V_{\text{eff}}\right)\phi = E\,\phi$$

Here $V_{\text{eff}}$ is defined as the **Effective Potential** (including inaccuracy due to ignoring interactions)

Since we know the equation

$$E\left[\{\Psi_i\}\right] = E_{\text{Known}}\left[\{\Psi_i\}\right] + \mathbf{E_{XC}[\{\Psi_i\}}$$

$$E_{\text{Known}}\left[\{\Psi_i\}\right] = T + \hat{V}_{ne} + \hat{V}_{ee} + \mathbf{E_{XC}[\{\Psi_i\}}$$

Considering the exchange correlational functional, since energy is functional of electron density and X-C is a part of energy, therefore X-C functional is dependent on the Electron Density Distribution.

Exchange correlational potential [90] is defined as

$$\frac{\delta E_{XC}(r)}{\delta(\rho(r))} \qquad \text{.............. 4.16}$$

## 4.2.1　　Self-Consistency of Kohn Sham Equation

$$[-\frac{\hbar^2}{2m}\nabla^2 + \hat{V}(r) + \hat{V}_H(r) + \hat{V}_{XC}(r)]\, \phi_i = \varepsilon_i\, \phi_i \qquad\qquad ............... \textbf{4.17}$$

Here in above equation $\hat{V}_H(r)$ is electron-electron coulomb interaction and defined as **Hartree – Potential**. It is given as

$$\hat{V}_H(r) = e^2 \int \frac{\rho(r\prime)}{r-r\prime} \qquad\qquad .......... 4.18$$

Whereas
$$\rho(r) = 2\sum \phi_i{}^*(r)\, \phi_i\, (r) \qquad\qquad ............. 4.19$$

To calculate the wave function $\phi_i$ (r), Hartree Potential as well as electron density should be known. But to know the electron density, Kohn Sham equation should be answered. Hence it is a repetitive procedure. Once the repetition is started with the electron density, the Kohn Sham equation corrects itself. That is why it is called that **Kohn Sham equation is self-consistent** [90]
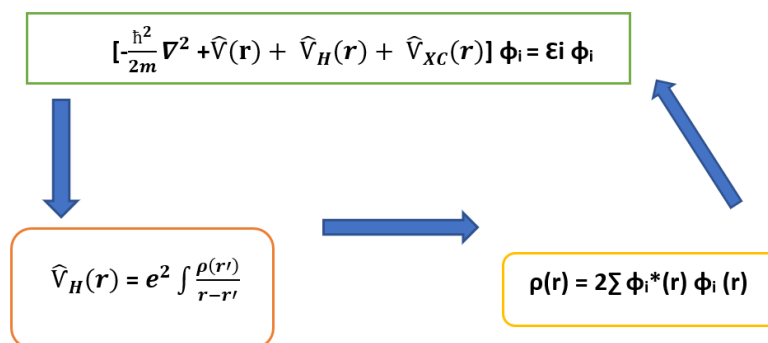


**Fig 4.1** Self-Consistency of Kohn Sham Equation

# 4.3 Exchange Correlational Functional

**Exchange Correlational Functional** consists of all the quantum aspects not incorporated in known term. All the unknown parts of the energy are included into EC functional which includes the quantum mechanical part of electron-electron interaction, the alteration for self-interaction and the kinetic energy that is not included in non-interacting reference system. The **Kohn Sham scheme** described above was to give exact solution of Kohn Sham equation. Different approximations are used for finding the exchange correlational functional. Till now no other approximation has been used other than Born- Oppenheimer approximation. The most widely used approximations for this are Local Density Approximation (LDA), Local Spin Density Approximation (LSDA) and Generalized Gradient Approximation (GGA)

# 4.3.1 Local Density Approximation (LDA)

The most widely used approximation used for solving exchange correlational functional is Local Density approximation (LDA) and Local Spin Density approximation (LSDA)

The most successful approach, LDA is based on the simplest electron distribution that is homogenous electron gas (HEG). In this approximation, the exchange corelation energy at each point in the system is equal as that of HEG of same density.

$$E_{XC}^{LDA} = \int \rho(r) \, \varepsilon_{XC}(\rho) \, dr$$

The exchange-correlation potential for LDA is determined by taking the rate of change of the exchange-correlation energy

$$V_{XC}^{LDA} = \frac{\delta E^{LDA}_{XC}}{\delta \rho(r)} = \varepsilon_{XC}(\rho) + \rho(r) = \frac{\delta \varepsilon^{LDA}_{XC}}{\delta \rho(r)}$$

LDA is the only approach where XC functional can be derived exactly. This approximation gives bond lengths and the geometries of molecules with accuracy of 1%. it is useful for the systems where density varies slowly.

## 4.3.2    Local Spin Density Approximation (LSDA)

The local spin-density approximation (LSDA) is a generalization of the LDA that includes spin polarization of the electrons into the functional for more accurate results. The density comprises of two parts: spin up density of electrons $\rho\alpha$ and the spin down density of electrons $\rho\beta$

$$E_{XC}^{LSDA} = \int \rho(r)\, \mathcal{E}_{XC}(\rho)\, (\rho_\alpha(r)\, \rho_\beta(r))\, dr$$

In this approximation, the spin polarization of a system after the splitting of spins is given as:

$$\xi(r) = \frac{\rho_\alpha(r) - \rho_\beta(r)}{\rho_\alpha(r) + \rho_\beta(r)}$$

For **paramagnetic system** since spin densities for both spin up and down are equal therefore $\xi(r)=0$, whereas for a **ferromagnetic system** the spin up and spin down states are split up which gives $\xi(r)=\pm 1$. LSDA is mostly used for the determination of magnetism and finding the type of magnetism in a system

But LDA and LSDA are not good when it comes to the calculation of energies. Just as LDA fails under rapid changes in density of molecules whereas LSDA assumes that the electron density is the same everywhere in the system. To overcome this there is another approximation mentioned that is Generalized Gradient Approximation (GGA).

## 4.3.3    Generalized Gradient Approximation (GGA)

 For upgrading the LDA, the step taken includes exchange-correlation impact of every microscopic volume not only reliant on the regional density in that volume, but also considering the density of the neighbouring volumes. In simple words, the gradient of the density is considered in this approximation. Hence it is therefore called as Generalize Gradient Approximation (GGA).

$$E_{XC}^{GGA} = E_{XC}\,[\rho(r),\, \nabla\rho(r)]$$

Where $\rho(r)$ is electron density and $\nabla\rho(r)$ is the density gradient. The exchange corelation potential for GGA is given as:

$$V_{XC}^{GGA}(r) = \left[ \frac{\delta f_{XC}^{GGA}}{\delta \rho(r)} - \frac{\delta f_{XC}^{GGA}}{\delta \nabla \rho(r)} \right]$$

The results obtained by solving KS equations using GGA are much better than the ones obtained through LDA or LSDA. Some of the GGA's that are described by different scientists and revised as well are mentioned:

➢ Langreth-Mehl 1983 (LM) [99]

➢ Perdew-Wang 1986 (PW86) [100]

➢ Becke-Perdew 1988 (BP) [101]

➢ Perdew-Burke-Ernzerhof 1996 (PBE) [98]

➢ Revised Perdew-Burke-Ernzerhof 1999 (RPBE) [103]

➢ Wu-Cohen 2006 (WC), [104]

This approximation is found exact most of the times but still not for every property. It has restricted general implementation. Therefore, for more precision the Meta GGA (MGGA) is produced that considers the semi-local evidence of the density or orbitals that are occupied.

# 4.3.4 Exchange-Correlation functionals Beyond LDA and GGA

The approximations for finding exchange correlation functional are not only till GGA and LDA but beyond this we have the hybrid functionals and Hubbard potential as well.

**Hybrid functionals** are defined as combination of two functional. We can take example of B3LYP which is a combination of BP and LYP GA functional, whereas PBE is a combination of Hartree exchange energy, PBE-GGA exchange energy and PBE-GGA correlation energy.

**Hubbard potential** were introduced after the failure of GGA and LDA functionals to calculate some properties of compounds like Mott insulators and magnetism in compounds with d and f orbitals. This led to the use of Hubbard potential in DFT, which includes the missing measures of the coulombic on-site interaction. The Hubbard potential was added to KS-DFT later by Anisimov et al. in 1991 [92]. Adding this potential to KS-DFT, bridged the gap between DFT and Hubbard potential to be able to calculate magnetism and other properties correctly. Hence the functional form was changed to LDA+U, GGA+U etc. where U indicates the Hubbard potential.

# 4.4    Wien2k

In this thesis Wien2k, a computer program is used for DFT calculations. This software package is coded in FORTRAN 90 and needs a UNIX-type operating system since the programs are linked together via C-shell scripts. The inaugurators of Wien2k program are Peter Blaha and Karl Heinz Schwarz of the 47 institute of Materials Chemistry, Vienna University of Technology [93]. This software was first released in 1990's referred as Wien93, Wien95 and Wien97 whereas Wien2k is its latest updated version [94] WIEN2k allows users to compute different properties of a structure applying the FLAPW method for the basis set. The choice of basis set and plan wave method is discussed further. While the simulations method and the different properties that can be calculated through WIEN2k are also described.

## 4.4.1    Choice of Basis Set and Wave Function

Different computer programs are used for solving the DFT equations, but they vary in the basis sets. Some use LCAO (linear combination of atomic orbitals) method for solving structure whereas some use Gaussian or Slater type orbitals (GTOs or STOs). Muffin Tin Approximation (MTA) is used where the potential and charge density inside the atomic sphere are taken to be spherically symmetric and for outside the sphere has a constant value for atoms in the crystal. Calculation of properties dependent on the density near the nucleus is described by electron wave function. Three basic schemes have been suggested for the plan wave functions i.e., Augmented Plane Wave (APW), Linear Augmented Plane Wave (LAPW) and Augmented Plane Wave with local orbitals (APW+LO) [96]

Different methods that have been described above have their own benefits or drawbacks when it comes to processing various quantities.

## 4.4.2    Augmented Plane Wave (APW)

In 1937, APW method was developed by Slater in which MTA is used, such that the potential near the nucleus and wave function is the same as the one inside the atom but for the interstitial positions the potential and wave functions are consistent and level. [97] Based on this analysis the space in a combination is partitioned into in two regions i.e., the non-intersecting spheres that make up the muffin tin and the overlapping spherical area is considered as the interstitial

region shown as region I and II in figure 4.2. Where for the expansion of muffin tin region, the radial solutions of the SWE are considered.

$$\Psi(\mathrm{r}) = \begin{cases} \sum_{lm} A_{lm} u_l(r) Y_{lm}(r) & r \in I \\ \frac{1}{\sqrt{\Omega}} \sum_G C_G e^{i(G+k).r} & r \in S \end{cases}$$

In above equation, wavefunction $\psi$, $\Omega$ is the cell volume, and $u_l$ gives the normal solution of equation

$$\left[ \frac{d^2}{dr^2} + \frac{l(l+1)}{e^2} + (V(r)) - E_l \right] r u_l(\mathrm{r}) = 0$$

C$_G$ and $A_{lm}$ are coefficients for expanding the wave function, $E_l$ is a parameter, V is the spherical component of the potential in the region I.
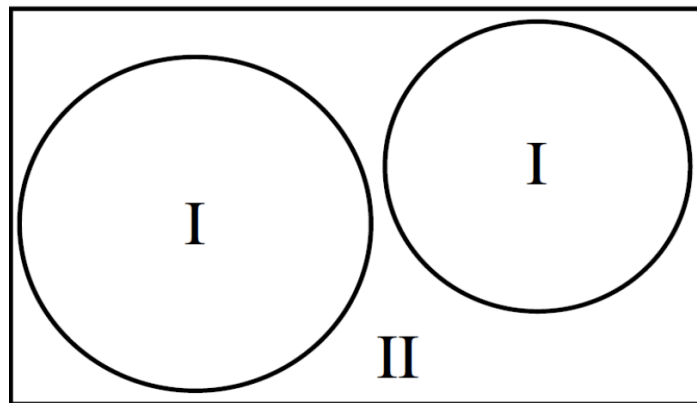


**Fig 4.2** Atomic muffin tin region I and Interstitial region II

However, the drawback of APW method is that the energies are not the same on the bounties as $ul(r)$ is zero on the boundary which will be a problem in general for elements with d and f orbitals. [98] Moreover, an additional problem using APW is its extension to a general crystal potential and removing the limitation of MTA [99]. To overcome these disadvantages, Anderson, and Abraham et al [100,101] gave the linearized plane wave methods called as **Linear Augmented Plane Wave method (LAPW)**

### 4.4.3     Linear Augmented Plane Wave method (LAPW)

The LAPW approach is the latest precise method for achieving electronic structure calculations for crystals. Based on the DFT for finding exchange and correlation it considers the LSDA approach. Like the other energy-band methods, this LAPW method is a technique for finding the solution to the Kohn-Sham equations for knowing the ground state density, total energy, and the eigenvalues of a crystal by establishing a basis set which fits according to the problem. In this method, the unit cell is divided into two regions, atomic spheres centred on the atomic sites (1) and an interstitial region (2) as seen from (figure 4.4)

In this method, linear combinations of radial functions, $ul(r)Ylm(\hat{r})$ and their rate of change with respect to the linearization parameters for inside the spheres, are used as basic functions, $El$. The $ul(r)$ is the same as used in the APW method with fixed energy $El$. The equation is modified as:

$$\psi \; (\text{r}) = \begin{cases} \sum_{lm}[A_{lm}u_l(r) + B_{lm \; U_{l'}(r)}Y_{lm}(r) & r \in I \\ \frac{1}{\sqrt{\Omega}}\sum_G C_G e^{i(G+k).r} & r \in S \end{cases}$$

In equation above, $B_{lm}$ is the coefficient for the energy derivative and is similar in meaning to $A_{lm}$. For the interstitial region of LAPW, the wave function is the same as that for APW. Only the correction is done mainly to inside sphere wave function.

### 4.4.4     APW+LO and LAPW+LO

Besides APW and LAPW method, there is one more extension can be added the correction to this method more efficient. This results when one utilizes the traditional APW basis, but with ul (r; $El$) at a fixed energy $El$ to keep the linear eigenvalue problem and then adds a new local orbital ($lo$) to have enough variational flexibility in the radial basis functions. Now the three functions $u_l(r)$, $u_l(r)$ and $u_{lo}(r)$ are all present together for the muffin tin sphere part of the wave function, while making sure that the derivative of local orbital is zero at the boundary. Moreover, though LO was introduced for treatment of semi-core electrons, the LAPW+LO scheme introduces correction to the electrons present in the higher states as well. The LAPW+LO basis functions are described as

$$\psi_{l_0}(r) = \sum_m [A^{l_0}_{lm} u_l(r) + B^{l_0}_{lm} u_l'(r) \, Y_{lm}(r)]$$

$A^{l_0}_{lm}$ and $B^{l_0}_{lm}$ are picked such that the boundary condition for local orbitals in MTA is satisfied.

## 4.4.5   The Full Potential LAPW (FP-LAPW)

The MTA was normally introduced in the 1970s and performs relatively well in tightly packaged systems. However, in case of covalently bonded solids and open or layered structures, MTA was found to be inappropriate approximation that precedes to serious differences with experiment. To avoid these estimates and for better calculations in all these cases a full-potential therapy is crucial in which charge density and potential density are expanded using the Fourier Series and lattice harmonics for interstitial and inside sphere calculations, respectively.

The combination of full potential scheme with the LAPW method gives us the FP-LAPW method, where FP is used in LAPW method instead of MTA. Full potential scheme treats the structure without giving it any specific shape i.e., spherical [102,103]. This simplification can be achieved by relaxing the constant interstitial potential $V_{Io}$ and the spherical MTA potential $V^L_{MT}(r)$ by the inclusion of interstitial potential $\sum_G V^G_I e^{iG.r}$ and the other terms inside the muffin-tin spheres:

$$V(r) = \begin{bmatrix} \sum_G V^G_I \, e^{iG.r} & r \in I \\ \sum_L V^L_{MT}(r) & r \in S \end{bmatrix}$$

FP-LAPW is the most precise methods for defining electronic structures for crystals by unravelling the Kohn-Sham equations of DFT. FP-LAPW is employed in the newest version WIEN2k to know about crystallographic properties on the atomic scale whereas the alternate basis set (APW+lo) is used for the chemically important orbitals, and LAPW is used for the others.

# 4.4.6        Simulation and Applications

Simulation can be run WIEN2k software package by making sure that WIEN2k software has been successfully installed on Linux operating system. After successful installation, different structures and materials can be simulated. However, in this latest updated version a graphical user interface (GUI) is also available for new users. The first step in calculating properties to simulate a structure by using the space group and atomic constants. Then proceed towards initialization where input files are generated. Afterwards according to the requirement, different commands are given to calculate the properties and then the output files are analysed for the results. [104]

 Kohn-Sham DFT is the popular method for computing the electronic structure of matter and its properties.  DFT can be used for analysing atomic structures, bulk structure, 2D surfaces and slabs. Some applications of DFT

- With the overall energy being calculated, the steadiness of various phases can be processed using DFT.
- Studying the electron density describes about the amount of charge transferred between the atoms in the material
- The band structure of the most complex materials can be obtained by using DFT and then the direct and indirect bandgaps can be calculated for further study
- The DOS of any material can be observed, including the partial DOS due to any orbital i.e., s, p, d, f,
- The optical properties of a material are studied by calculating the optical parameters of a material such as refractive index, optical conductivity, optical reflectivity, optical dielectric constant.
- The magnetic properties of different samples can be determined and calculated i.e., magnetic moment, the spin up/down density.

# Chapter 05

# Results and Discussion

## 5.1 Experimental Discussion

### 5.1.1 XRD Analysis

XRD is a technique that is used for the structural analysis of compounds and to observe the presence of different materials that are deposited on compound. The XRD pattern of $Nb_2C$ MXene and it adsorbed compound is shown in Figure 5.1. Both the patterns are compared, and results are deduced.

The diffraction pattern of Ni-adsorbed $Nb_2C$ shows that it is slightly different from the pattern of functionalized $Nb_2C$ MXene. No extra external peak related to any of the reactants confirms that Ni-adsorbed $Nb_2C$ is successfully synthesized. The peaks for Ni adsorbed MXene are observed at 33.4° and 59.5° and agree with the diffraction pattern of pure $Nb_2C$. The change in pattern is observed at 23°at plane (004). The decrease of peaks however indicates the crystallinity of the structure decreases more with increase of Nickel and results with disappearing of diffraction peaks shown for parent compound i.e., $Nb_2C$ MXene.

For $Nb^{2+}$, the ionic radius is 0.07nm whereas for the dopant $Ni^{2+}$ the ionic radius is 0.069 nm. The ionic radius of $Ni^{2+}$ is in close approximation to that of $Nb^{2+}$, which indicates that the variations in diffraction pattern agree with the size of crystallite. The decline in the size of crystallite is due to the disturbance in the host $Nb_2C$ lattice by the presence of $Ni^{2+}$ ions. The replacement of $Ni^{2+}$ ions in the interstitial position of host MXene lattice sites would disturb the intensity of the interstitial sites of $Nb_2C$ which causes the peaks broadening. [105] The excuse of adsorption of Ni $^{2+}$ ions on the surface of $Nb_2C$ is because of MXene negative potential surface caused by the presence of negative surface terminations (–O, –OH, –F). Therefore, $Nb_2C$ MXene has a great capability to invite positively charged $Ni^{2+}$ ions. Ion exchange phenomenon may also take place at the surface between the $Ni^{2+}$ ions and negative surface terminations which results in formation of Ni-$(OH)_2$ oxides as shown in the XRD pattern.[106]
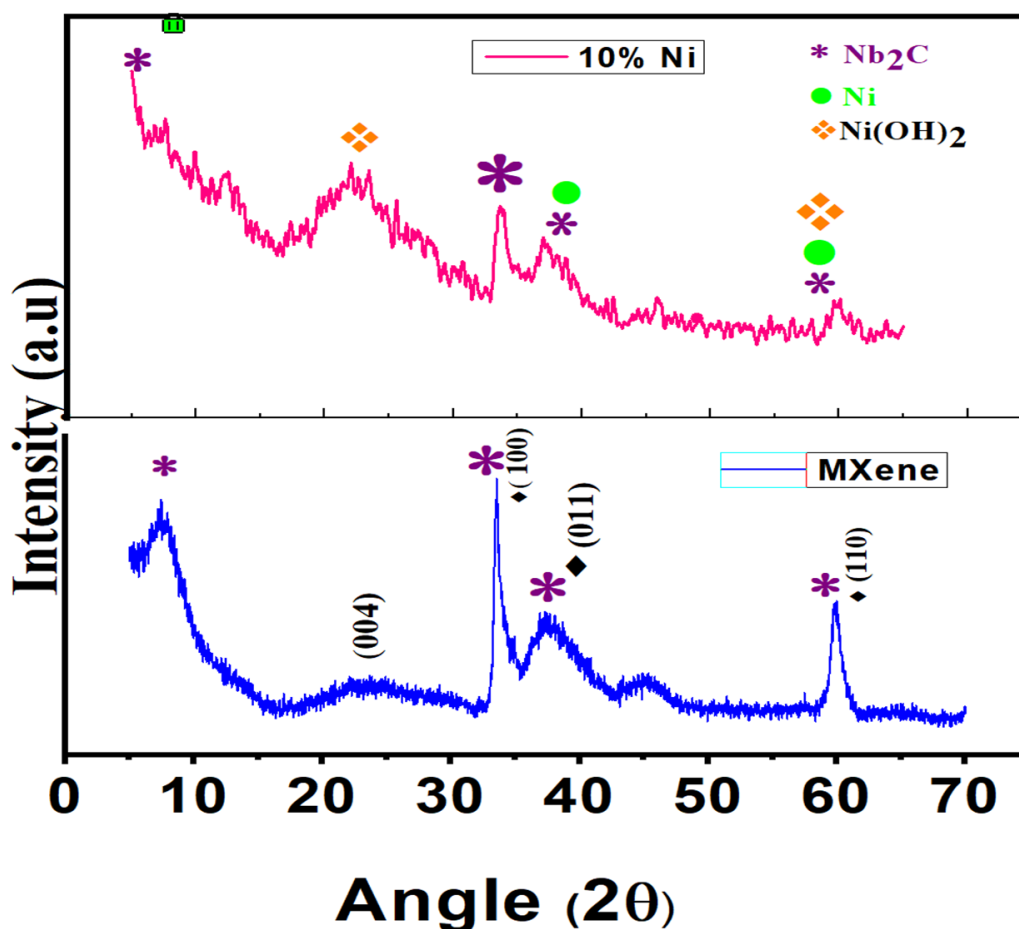
**Fig 5.1** XRD Spectrum for $Nb_2C$ MXene and its Adsorbed Compound Ni-$Nb_2C$

## 5.2    Theoretical Discussion

For the understanding of $Nb_2C$ functionalized MXene and its adsorbed compound the magnetic behaviour of these synthesized compounds is discussed in this thesis. The two compounds were analysed and were studied computationally using DFT.

First the structure for both compounds, i.e., $Nb_2C$-O-F and Ni bonded $Nb_2C$-O-F were simulated using the DFT software package i.e., Wien2k. Then super cells were created and optimized. The stable structure was analysed for the magnetic behaviour.

For the study of $Nb_2C$ MXene, computational analysis is done by FP-LAPW method applied in WIEN2k. The electronic structures, band gaps and DOS plots per eV were calculated, analysed, and are discussed below.

# 5.3　　　Nb₂C-O-F MXene

The Nb₂C-O-F structure is simulated by a supercell of slabs. Each slab comprises of five layers. The C layer is inserted between Nb layers whereas Oxygen and Fluorine atoms are inserted to the system as functional group to terminate the surface (Figure 5.2). A unit cell of Nb₂C-O-F consist of 4Nb atoms, 2 atoms of Carbon, 3 Oxygen atoms and 1 Fluorine atoms. The proposed structure is expanded into 2×2×1 supercell and optimized. The slab thickness is taken 5.2 Å. In the supercell, these slabs are disconnected by vacuum of about
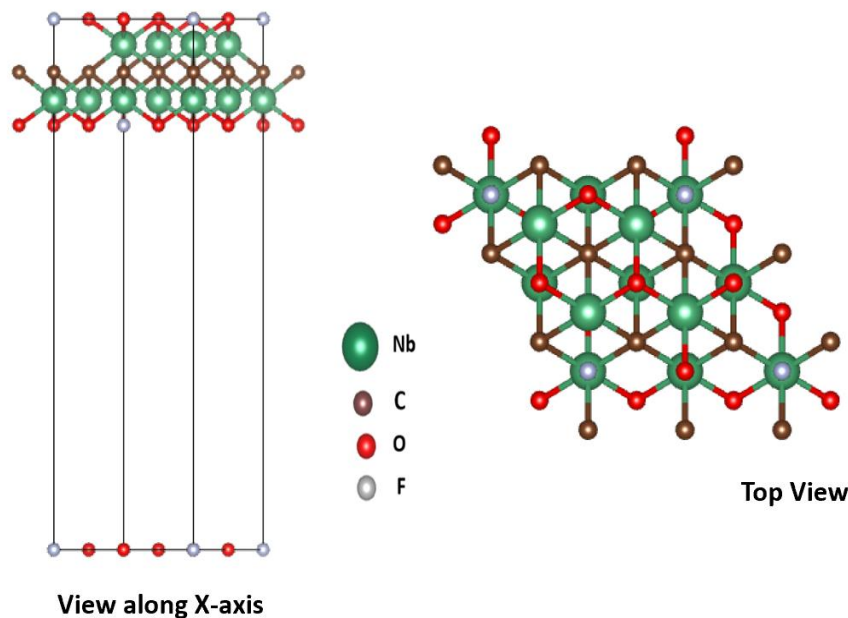17.5 Å.



**Fig 5.2** Optimized simulated structure image of Nb₂C-O-F

## Optimization and Minimization

The structure of Nb₂C-O-F was optimized and minimized at about 500 k-points with a k-mesh of 7x7x7 in the irreducible Brillouin zone (IBZ). The unit cell for Nb₂C-O-F after the optimization and minimization is shown in figure. Nb₂C-O-F has hexagonal structure with the space group 1_P1. The lattice parameters (taken in Bohr units) are a=b = 11.785882 and c = 42.707811 and $\alpha = \beta = 90°$ and $\gamma = 120°$. The RMT radii considered are　1.92 a.u. for Nb atoms, 1.78 a.u. for O atoms, 1.82 a.u. for F atoms, 1.73 a.u. for C atoms while the scf calculations were performed by 64 k-points with a k-mesh of 6 ×6× 1 in the IBZ with the

energy convergence criteria taken to be $10^{-5}$ Ry and charge convergence to be $10^{-4}$ e.

## 5.3.1 Electron Density

Electron density is a useful quantity for the analysis and understanding of materials. It helps to understand the chemical bonding. The electronic properties of functionalized Nb₂C MXene are also studied computationally as shown in Figure. The density of Nb is found to be more than that of carbon as it has filled 3d orbital and partially filed 4d orbitals whereas C has only partially filled p orbital. From figure, C shows large electron density image because the p-orbital is shown spreading where as in Nb the electron density image is smaller as the energy is condensed within its orbitals. From the temperature scale, we can see that Nb has higher electron density then carbon. Hence presence of niobium atom modifies the electron density and strengthen the bond.
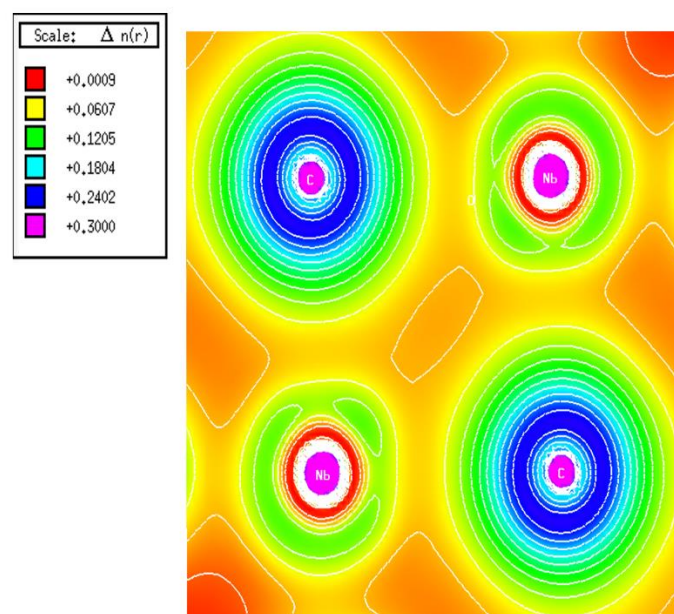


**Fig 5.3** Electron density of simulated structure of functionalized Nb₂C

## 5.3.2 Band Structure

Band structure of any compound or element describes about the nature of material regarding its conduction i.e., metallic, insulating, or semi-conducting. Figure shows the band structure for Nb₂C-O-F MXene. It can be predicted from the band structure that this material has metallic behaviour since the band gap is zero. It has been predicted from literature that most of

functionalized MXene have metallic nature. [62] The result shows that functionalized $Nb_2C$ MXene is metallic and here the Fermi energy is all caused by d orbital of M transition element i.e., Niobium.
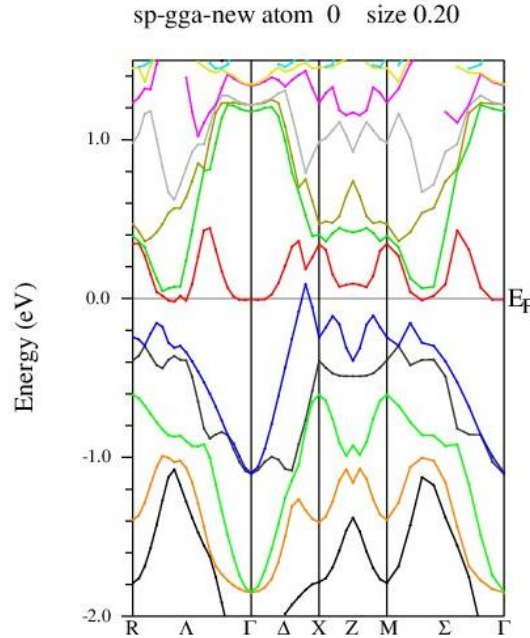


**Fig 5.4** Band structure of minimized $Nb_2C$-O-F MXene

## 5.3.3       Density of States (DOS)

To examine the contribution of each element in the density of states, a DOS plot for $Nb_2C$-O-F is shown below. The DOS plot of spin up is mirror image of spin down as in Figure 5.5. F is totally spread in valence band with no existence in conduction band. C also shows its peak in valence band. From the plot in the range -10 to -6 eV, which is the valence band, all the elements are contributing and giving total DOS plot in this region. This shows that all atoms in super cell are strongly bonded and give the total DOS. No band gap can be seen from the plot since the states are overlapping and hence metallic behaviour of this can also be proved from this DOS plot.

Nb peaks are present in valence and conduction band and occupies the range from -3 to 7 eV. But the highest peaks are visible in conduction band Nb and the total DOS increases with high peak in this range, this shows that magnetic behaviour in $Nb_2C$-O-F is due to Nb atoms.
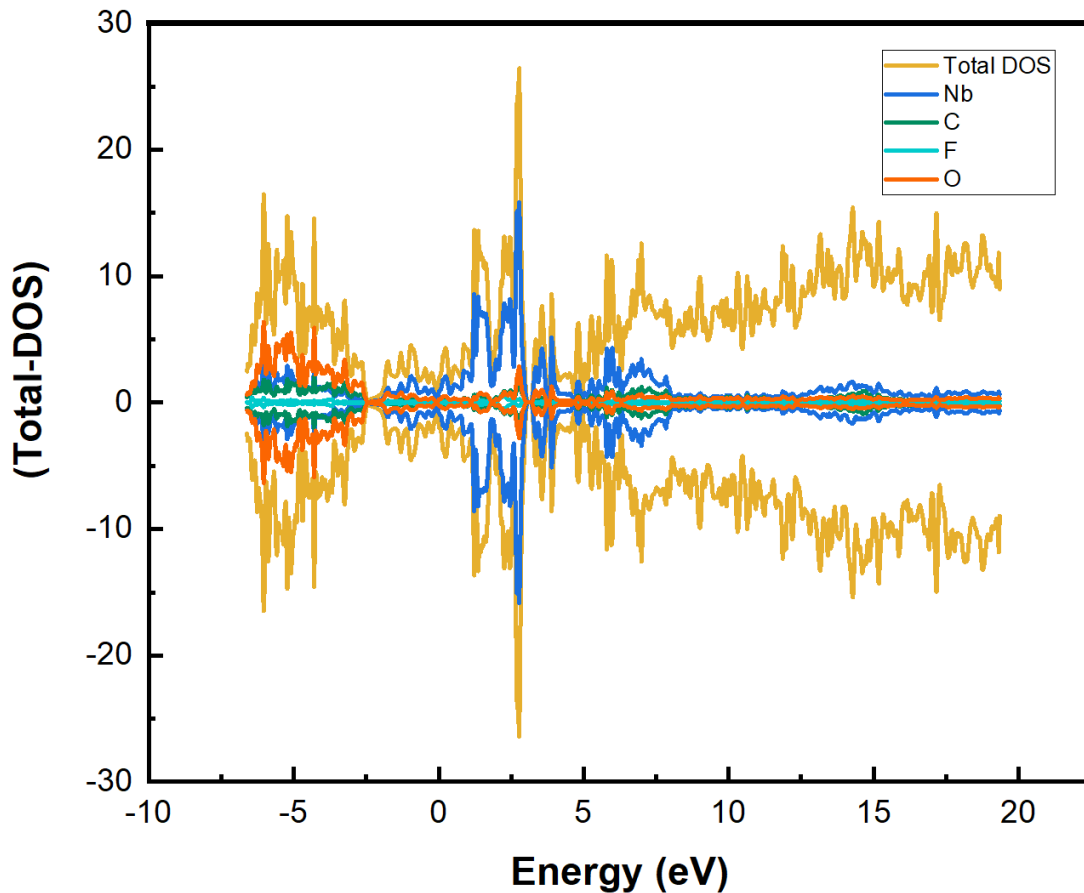
**Fig 5.5** TDOS for $Nb_2C$-O-F MXene

## 5.3.4 Partial Density of States (PDOS)

Figure 5.6 shows the plot for PDOS of $Nb_2C$-O-F MXene using the spin-GGA approximation with 64 k-points. The PDOS plots for the subshells of Niobium, Fluorine and Oxygen are shown below. From the PDOS plot of Nb, we can see that the highest peaks are present within the conduction band from 0eV to 5 eV for Nb-d orbital. By comparison of this conduction region (from 0-5eV) in all other elements PDOS plot, F-s and F-p orbitals, C-p orbital, and O-p orbital with less contribution show density of states. This means that these atomic orbitals are overlapping within the conduction region with the major Nb-d orbital. As a result, this overlapping results in hybridization in functionalized $Nb_2C$-O-F. By hybridization we mean that new states are generated for the availability of electrons and this hybridization is

responsible for the magnetic behaviour in Nb2C-O-F MXene. The region in conduction band from 5 to 20 eV also shows that the overlapping between all atomic orbital is taking place resulting in hybridization.
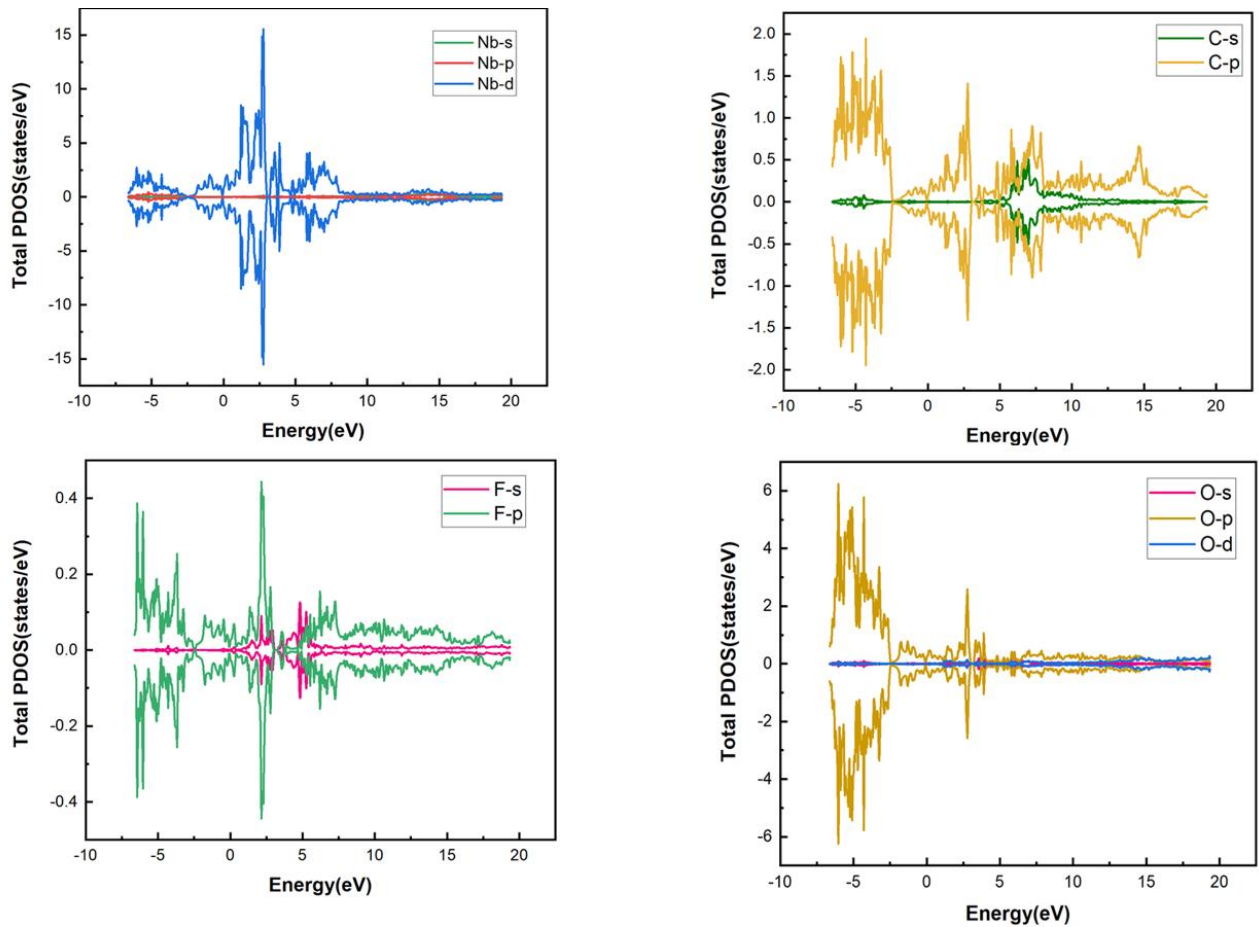


**Fig 5.6** Partial Density of States for all the Elements in Nb$_2$C-O-F

The total PDOS plot is shown in Fig 5.7. As seen from the plot, the Nb-d, F-s, and O-p orbitals show large contribution within the valence band whereas the largest contribution in the conduction band is given by the Nb-d and Oxygen-p orbitals. The overlapping of Nb-d, O-p along with O-s and F-p can be seen in the range of conduction band from 4eV to 20 eV. This overlapping gives the result of hybridization in the functionalized Nb$_2$C-O-F MXene. As overlapping is small so less hybridization is existing in this structure.

**Fig 5.6** PDOS plot for Nb$_2$C-O-F MXene

# 5.4 Adsorbed and Doped Structures

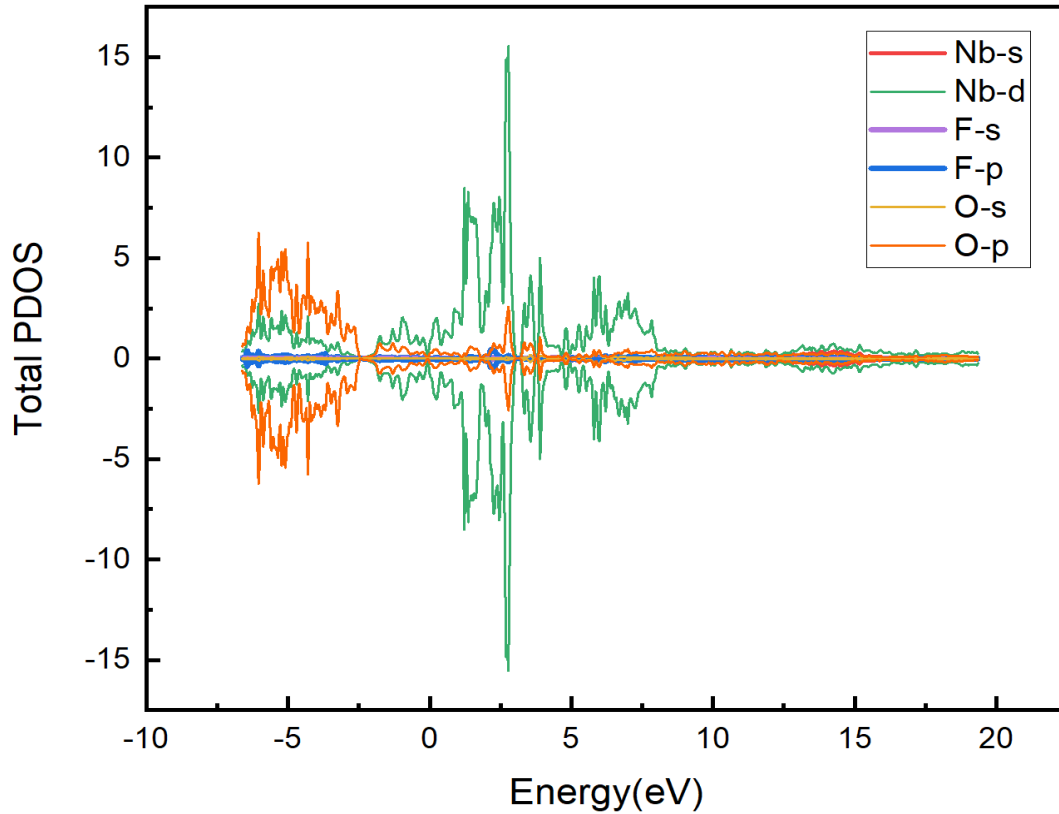The two structures i.e., Adsorbed and Doped compounds were simulated using WIEN2K software for the understanding of Nickel incorporated Nb$_2$C MXene. The doped structure consisted of total 20 atoms and the adsorbed structure consisted of 21 atoms. The unit cell of 2× 2 for both simulated structures are shown in figure below. Ground state energy for adsorbed and doped structure calculated was -65777.5818 Ry and -58136.5490 Ry respectively. Energy convergence criteria used for the scf was such that the differences in the total energies do not exceed $10^{-5}$ Ry. Since more negative the minimization energy more stable is the structure. Hence the adsorbed structure was found more stable than the doped one. Therefore, all the characteristic analysis for electric and magnetic properties was performed for the adsorbed structure by using DFT software Wien2k.

| DOPED STRUCTURE | ADSORBED STRUCTURE |
|---|---|
| 7 Nb | 8 Nb |
| 1 Ni | 6 O |
| 6 O | 2 F |
| 2F | 4 C |
| 4 C | 1 Ni |
| **Total:** 20 | **Total:** 21 |

**Table.2** Adsorbed and Doped Structure atoms
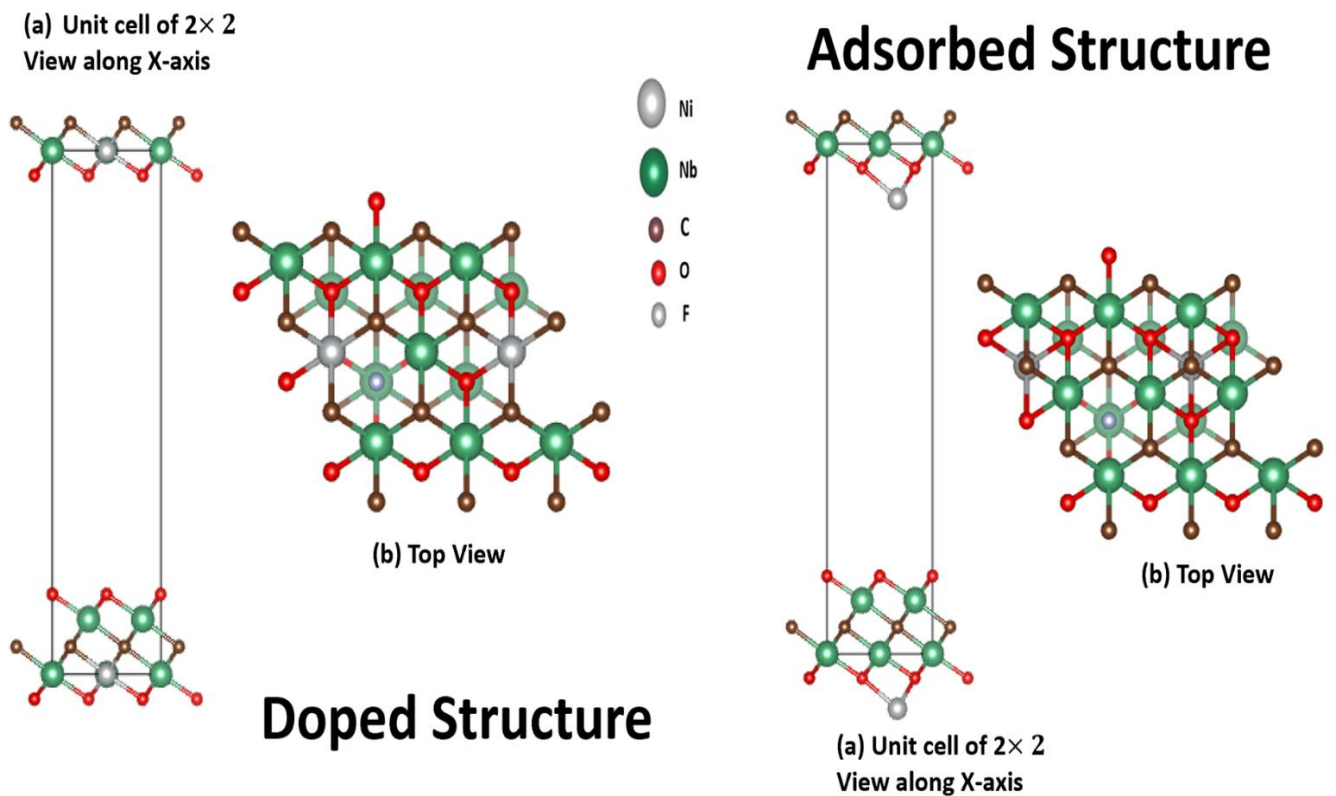


**Fig 5.6** Doped and Adsorbed Structure unit cell

## 5.5　　　　Ni-Nb₂C-O-F MXene

**Structure**

The Ni-Nb$_2$C-OF structure is designed consisting of supercell including slabs in similar as that of Nb$_2$C functionalized. The calculations are performed by GGA+ U exchange-correlation functional [63]. Here U indicates the Hubbard potential that includes the non-local corrections to the E$_{xc}$ functional. The wave functions in the interstitial regions are extended in plane waves, with the plane wave cut-off taken as R$_{MT}$ K$_{max}$= 7.0

$4 \times 4 \times 1$ supercell is simulated to analyse the steady structure for Ni adsorbed Nb$_2$C-O-F. The Ni-adsorbed compound has space group 81_1_P1 with the c-lattice parameter as 42.707792 Bohr. The RMT radii considered are 1.92 a.u. for Nb atoms, 1.78 a.u. for O atoms, 1.82 a.u. for F atoms, 1.73 a.u. for C atoms and 2.11 a. u for Ni atom. The wave functions inside the spheres are expanded in spherical harmonics up to the maximum angular momentum l$_{max}$ = 10

**Optimization and Minimization**

Optimization and minimization of the simulated structure was done by modifying the internal geometry of the system by modified tetrahedron integration scheme using 54 k-points in IBZ distributed as 6×6×3 Monk horst–Pack grid.

The internal geometry of compound is optimized such that the forces acting on each atom are less than 1 mRy/a.u. While the convergence criteria for the scf do not exceed $10^{-5}$ Ry for successive steps.
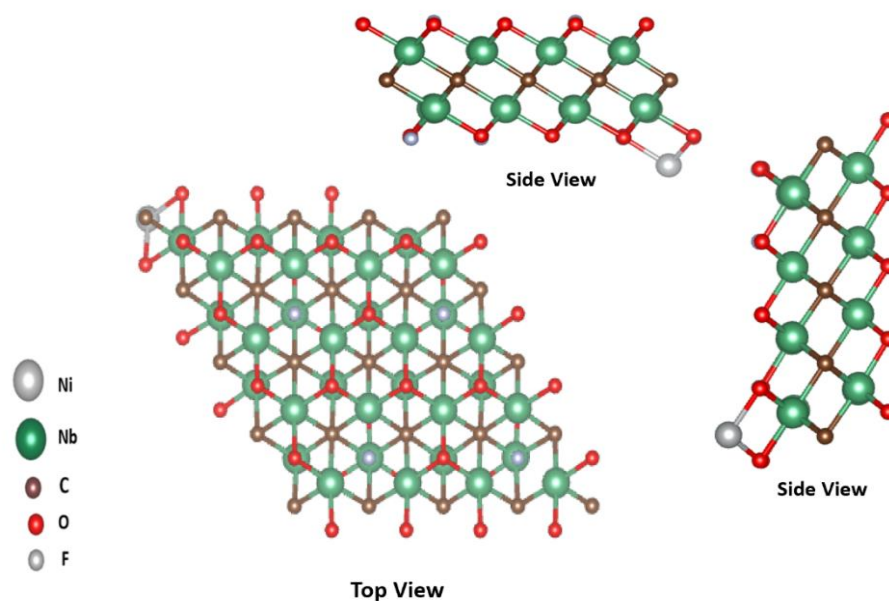


**Fig 5.7** Optimized and Minimized structure of Ni-Nb$_2$C-O-F

## 5.5.1 Band Structure

As already know that band structure of any compound or element explains the the scope of energy levels that electrons may have within it, as well as the ranges of energy that they may not have which we can be called as band gap. Band structure talks about the nature of material regarding its conduction i.e., metallic, insulating, or semi-conducting. From, the figure below, the Ni-adsorbed $Nb_2C$-O-F MXene is found to be metallic as it has zero band gap. As seen from the picture that the different energy levels are seen overlapping and crowding the fermi level which shows its metallic behaviour. The fermi energy is influenced by the d orbitals of niobium as well as the external element i.e., Nickel which means that the fermi energy is located at the d-bands of transition metal Nb and Nickel.
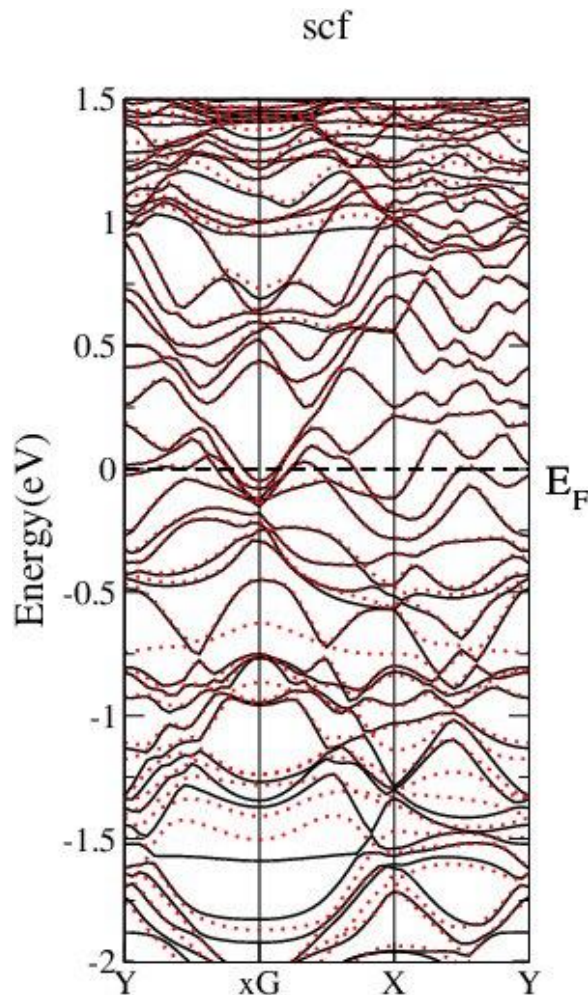


**Fig 5.8** Band structure of minimized Ni-$Nb_2C$-O-F MXene

## 5.5.2        Density of States (DOS)

DOS are stated as number of different states at a particular energy level that electrons are allowed to occupy. Figure shows that total density of states (TDOS) plot for the adsorbed compound Ni-$Nb_2$C-O-F MXene computed by using the spin-GGA+U where U= 6eV. The k-points taken were 150 with the k-mesh $6 \times 3 \times 3$.

Nickel is one of the elements that are ferromagnet at room temperature. When Ni is adsorbed on the MXene, it forms bond with Fluorine and Oxygen atom. It can be seen in figure below. DOS versus energy plot for Ni-Adsorbed MXene is shown below. The TDOS spin up and spin down seems not to be mirror of each other. This indicates the Ferromagnetic nature of the adsorbed material. DOS of Ni, Nb, C, O, F is shown. F is mainly in the region of -8 to -6 eV and totally limited in Valence band. -7 to -5 is the range in which the TDOS peak is the highest as all the elements are contributing to this range. In the range -2 to 0 eV the Density of states of Nickel for spin up and down can be observed which is totally different showing its magnetic behaviour. From the range 0 to 5 eV which is the conduction band, most of the TDOS is contributed by Nb in this range.

From figure, the difference in the intensity of peaks for spin-up and the spin down which indicates that the DOS/eV is dividing into both spins and hence resulting in magnetism which will be verified from the values of magnetic moment.
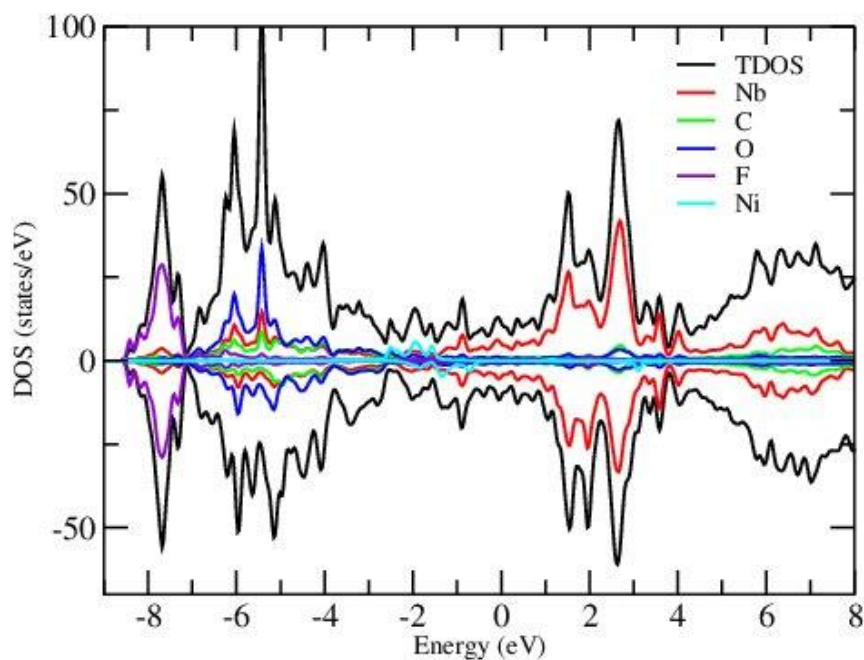


**Fig 5.9** TDOS for Ni-$Nb_2$C-O-F MXene

### 5.5.3 Magnetic Moment

Magnetism in adsorbed compound i.e., Ni-Nb$_2$C-O-F has not been studied till now where as functionalized Nb$_2$C MXene has been predicted to be diamagnetic in recent publication. [72] The total magnetic moment of Nb$_2$C-O-F is found negative i.e. −0.00027μB in our case which confirms the diamagnetic behaviour according to the literature. It is observed that negative magnetic moment is mainly contributed entirely by the Nb-atoms as seen from plot of magnetic moment (Fig 5.10) within the range of 0 to 8 atoms

The total magnetic moment calculated for the adsorbed MXene Ni-Nb$_2$C-O-F is + 1.01516 $\mu_B$ it is observed that O and Nb forms a bond with the nickel which effects magnetic moments. It can be seen (Fig 5.6), two oxygen atoms and one niobium atom form a bond with doped nickel. The magnetic moment calculated for these two O atoms, one Nb and Ni is mentioned in the table below. The magnetic moment for O and Ni is positive with large value which dominates the negative magnetic moment of Nb. Hence the negative magnetic moment from the Nb atom is generally decreased and a positive magnetic moment is revealed by all the Nb atom showing the Ferromagnetic behaviour. In simple words, it can be said that the switching of this magnetic behaviour and the change of superconducting to non-superconducting behaviour is reasoned due to the surface termination and the adsorption of Nickel atom.

Fig 5.9 shows the plot of magnetic moment for all the atoms in supercell which includes 31 Nb, 32 functional groups atoms i.e., O and F, 16 C's and 1 Ni atom, giving a total of 80. From the plot of magnetic moment for Ni-Nb$_2$C-O-F, the atoms from 30 to 45 and at the end after 75 shows clear high peaks for magnetic moment which shows the clear Ferromagnetic nature. This verifies that the adsorption of Nickel in Nb$_2$C-O-F MXene favours adsorption which alters the diamagnetic behaviour and superconductivity of functionalized Nb$_2$C into FM non-superconducting behaviour in Ni-Adsorbed Nb$_2$C MXene.

| Magnetic Moment | Nb 8 | Oxygen 36 | Oxygen 42 | Nickel 81 | Total |
|---|---|---|---|---|---|
| PBE -GGA + U | -0.00195 | 0.02249 | 0.02249 | 0.84300 | 1.01516 |

**Table.3** Magnetic moment for Ni-Nb$_2$C-O-F

Hence, summarizing the above analysis we can say that here we have observed the effect of adsorption and surface terminations in determining transition from diamagnetic-superconductive to ferromagnetic non-superconductive behaviour in simulated MXene and its adsorbed compound.
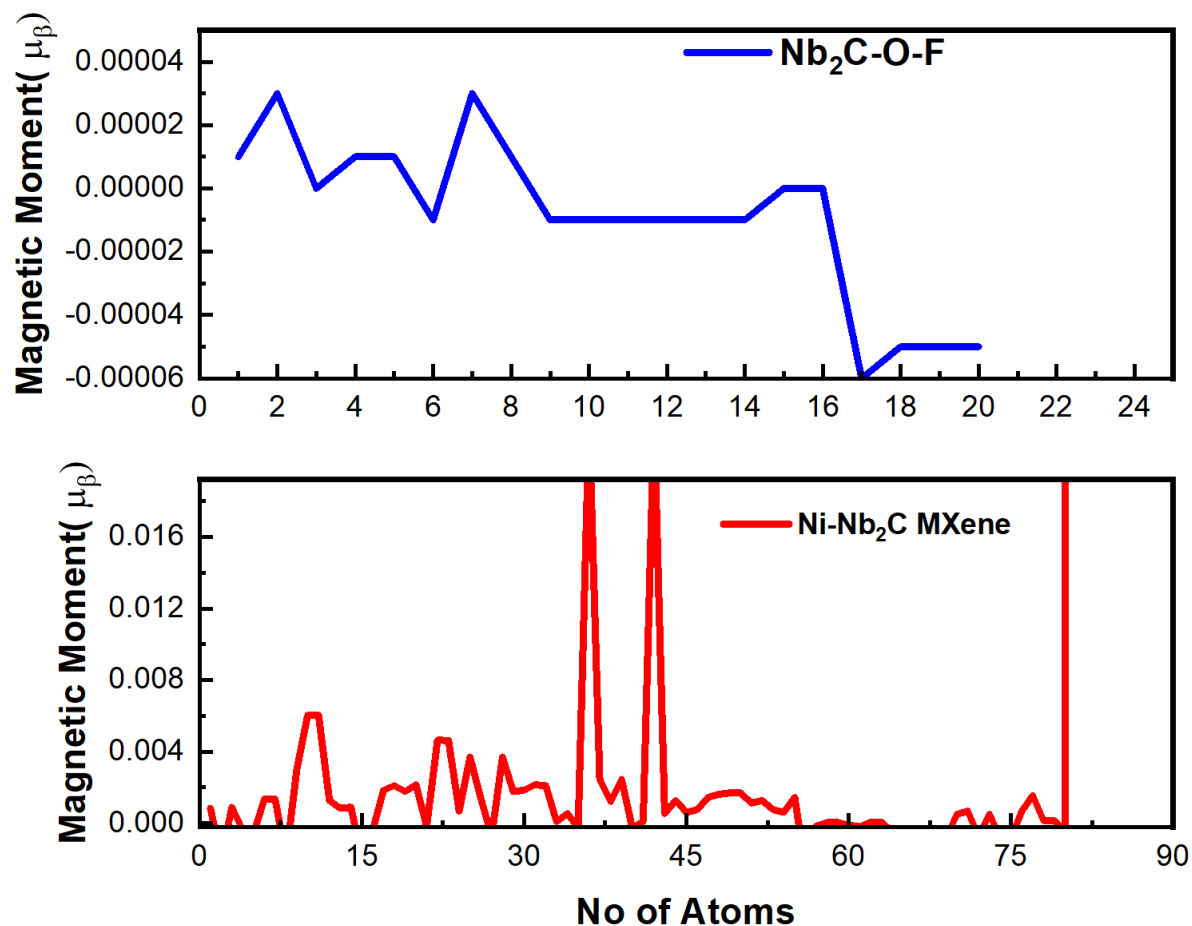


**Fig 5.10** Magnetic moment plot for simulated $Nb_2C$-O-F and Adsorbed compound Ni-$Nb_2C$-O-F

# Chapter 06

# Conclusion

In whole thesis, we have in theory analysed the electronic structural and magnetic characteristics of functionalized $Nb_2C$ and its adsorbed compound $Ni-Nb_2C$ MXene by applying the Density Functional Theory. The structure of both compounds was simulated by using DFT software package i.e., Wien2k Both the structures created were first optimized and minimized. The stable structures were analysed for the magnetic behaviour. For the study of $Nb_2C$ and $Ni-Nb_2C$ MXene, the computational analysis is done by FP-LAPW method applied in WIEN2k. The electronic structures, band gap and density of states (DOS) per eV were computed, analysed, and are discussed.

The structure of $Nb_2C$-O-F was optimized and minimized at about 500 k-points with a k-mesh of 7x7x7 in the IBZ. While the scf calculations were performed by 64 k-points with a k-mesh of 6 ×6× 1 in the irreducible Brilloiun zone (IBZ) with the energy convergence criteria taken to be $10^{-5}$ Ry and charge convergence criteria to be $10^{-4}$ e. The electron density of Niobium was found greater than that of carbon due to its filled 3d orbital and partially filled 4d orbital. The band structure showed the metallic behaviour of functionalized $Nb_2C$ with zero band gap. The DOS plot showed the strong bonding of all elements in the super cell. The magnetic moment calculated for $Nb_2C$-O-F is found to be $-0.00027\mu_\beta$ which is although a small value but confirms its diamagnetic behaviour.

Similarly, the structure simulated for $Ni-Nb_2C$-O-F was first optimized and minimized. $4 \times 4 \times 1$ supercell was used to analyse the steady structure for Ni adsorbed $Nb_2C$-O-F. Optimization and minimization of the simulated structure was done by modifying the internal geometry of the system by using 54 k-points in IBZ distributed as 6×6×3 Monk horst–Pack grid.

The inside structure of compound is optimized such that the forces acting on each atom are less than 1 mRy/a.u. Convergence criteria for the scf do not exceed $10^{-5}$ Ry for successive steps.

The band structure analysis showed metallic behaviour for this compound with zero band gap. The DOS plot graphed depicts the ferromagnetic behaviour along with non-superconductive nature which was further confirmed by the magnetic moment. The total magnetic moment

calculated for Ni-Nb$_2$C-O-F is $+1.01516\mu_\beta$. the diamagnetic superconducting behaviour of Nb$_2$C-O-F was converted to non-superconducting ferromagnetic nature due to the adsorption of Nickel ions on parent compound. The magnetic moment of adsorbent and surface terminations dominated the Nb magnetic moment and converted Ni-Nb$_2$C-O-F into ferro magnet.

## 6.1      Future Recommendations

In this thesis, although the work is done completely and digressively but still there some points that need to be focused. In case of magnetism, the Antiferromagnetic analysis can be checked for the adsorbed compound. For the better understanding of DOS plot the Partial density of states (PDOS) can be calculated that can help in better understanding of band gap and magnetic nature. All these calculations can be made by using DFT software. Moreover, the magnetic properties can be checked by using other exchange correlational functionals such as LDA and LSDA and compared with this current analysis.

# References

[1] Samer Bayda, Muhammad Adeel, Tiziano Tuccinardi, Marco Cordani, Molecules, 25, (2020) 112

[2] G. Yu, X. Xie, L. Pan, Z. Bao, Y. Cui, Nano Energy 2, (2013), 213

[3] M. Naguib, M. Kurtoglu, V. Presser, J. Lu, J. Niu, M. Heon, L. Hultman, Y. Gogotsi, M.W. Barsoum, Adv. Mater. 23, (2011) 4248

[4] Utic IZ, Fabian J, Sarma SD. Rev Mod Phys 76, (2004),  323–386

[5] Sinova J, Zutic I. Nat Mater 11 (5), (2012) 368–371

[6] Wolf SA, Awschalom DD, Buhrman RA, Daughton JM, Sv M, Roukes ML, Chtchelkanova AY, Treger DM Science 294, (2001) 1488–1495

[7] Liu C, Chen H, Wang S, Liu Q, Jiang YG, Zhang DW, Liu M, Zhou P. Nat Nanotechnol 15(7), (2020), 545–557

[8] Han W APL Mater 4(3), (2016), 032401

[9] Pesin D, MacDonald AH. Nat Mater 11(5), (2012), 409–416

[10] Drogeler M, Franzen C, Volmer F, Pohlmann T, Banszerus L, Wolter M, Watanabe K, Taniguchi T, Stampfer C, Beschoten B  Nano Lett 16(6), (2016), 3533–3539

[11] Han W, Kawakami RK, Gmitra M, Fabian J Nat Nanotechnol 9(10), (2014), 794–807

[12]  Alagarasi, AIntroduction to Nanomaterials Chapter 1, (2011), 76

[13] Gnach, A.; Lipinski, T.; Bednarkiewicz, A.; Rybka, J.; Capobianco, J.A.. Chem. Soc. Rev. 44, (2015)1561–1584.

[14] Khan, I., Saeed, K., & Khan, I. Arabian Journal of Chemistry. (2017).

[15] B Anasori, MR Lukatskaya, Y Gogotsi Nature Reviews Materials 2 (2), 1-17

[16] M. W. Barsoum and M. A. X. Phases, Properties of Machinable Ternary Carbides and Nitrides, Wiley & Sons, 2013

[17] **Anasori**, Babak, **Gogotsi**, Yury, Introduction to 2D Transition Metal Carbides and Nitrides (MXenes)

[18] B Anasori, MR Lukatskaya, Y Gogotsi - Nature Reviews Materials, 2017

[19] M. Naguib, O. Mashtalir, J. Carle, V. Presser, J. Lu, L. Hultman, Y. Gogotsi, and M. W. Barsoum, Two-dimensional transition metal carbides, ACS Nano 6(2), 1322 (2012)

[20] M. Kurtoglu, M. Naguib, Y. Gogotsi, and M. W. Barsoum, First principles study of two-dimensional early transition metal carbides, MRS Commun. 2(04), 133 (2012)

[21] Tang, X., Guo, X., Wu, W., & Wang, G. (2018). 2D Metal Carbides and Nitrides (MXenes) as High-Performance Electrode Materials for Lithium-Based Batteries. Advanced Energy Materials, 1801897

[22] Guo, Z., Zhou, J., Zhu, L., & Sun, Z. (2016). MXene: a promising photocatalyst for water splitting. Journal of Materials Chemistry A, 4(29), 11446–11452

[23] A.Iqbal,J.Kwonc M-K.Kim Materials Today Advances, ISSN: 2590-0498, Vol: 9, Page: 100124 Publication Year2021

[24] Li, X., Ran, F., Yang, F. et al. Advances in MXene Films: Synthesis, Assembly, and Applications. Trans. Tianjin Univ. **27,** 217–247 (2021)

[25] Xie, X., Chen, S., Ding, W., Nie, Y., & Wei, Z. (2013). An extraordinarily stable catalyst: Pt NPs supported on two-dimensional $Ti_3C_2X_2$ (X = OH, F) nanosheets for oxygen reduction reaction. Chemical Communications, 49(86), 10112.

[26] Wang, F., Yang, C., Duan, M., Tang, Y., & Zhu, J. (2015). $TiO_2$ nanoparticle modified organ-like $Ti_3C_2$ MXene nanocomposite encapsulating hemoglobin for a mediator-free biosensor with excellent performances. Biosensors and Bioelectronics, 74, 1022–1028

[27] K. Hantanasirisakul, Y. Gogotsi, Electronic and optical properties of 2D transition metal carbides and nitrides (MXenes), in: Advanced materials, 30, 2018, pp. 1804779

[28] C. Xu, L. Wang, Z. Liu, L. Chen, J. Guo, N. Kang, X.-L. Ma, H.-M. Cheng, W. Ren, Large-area high-quality 2D ultrathin $Mo_2C$ superconducting crystals, Nature Mater. 14 (2015) 1135.

[29] G. Gao, G. Ding, J. Li, K. Yao, M. Wu, M. Qian, Monolayer MXenes: promising half-metals and spin gapless semiconductors, Nanoscale 8 (2016) 8986–8994.

[30] H. Kumar, N.C. Frey, L. Dong, B. Anasori, Y. Gogotsi, V.B. Shenoy, Tunable magnetism and transport properties in nitride MXenes, ACS Nano 11 (2017) 7648–7655.

[31] Anasori, B., Lukatskaya, M. & Gogotsi, Y. 2D metal carbides and nitrides (MXenes) for energy storage. Nat Rev Mater **2,** 16098 (2017).

[32] Zhuoheng Bao; Chengjie Lu; Xin Cao; Chinese Chemical Letters, ISSN: 1001-8417, 2021

[33] Rina Ibragimova, Paul Erhart, Patrick Rinke, and Hannu-Pekka Komsa The Journal of Physical Chemistry Letters **2021** 12 (9), 2377-2384

[34] Ghidiu, M.; Lukatskaya, M. R.; Zhao, M.-Q.; Gogotsi, Y.; Barsoum, M. W. Conductive Two-Dimensional Titanium Carbide 'Clay' with High Volumetric Capacitance. Nature **2014**, 516, 78– 81

[35 ] Zhang, C. J.; Anasori, B.; Seral-Ascaso, A.; Park, S.-H.; McEvoy, N.; Shmeliov, A.; Duesberg, G. S.; Coleman, J. N.; Gogotsi, Y.; Nicolosi, V. Transparent, Flexible, and Conductive 2D Titanium Carbide (MXene) Films with High Volumetric Capacitance. Adv. Mater. **2017**, 29, 1702678

[36] Halim, J.; Cook, K. M.; Naguib, M.; Eklund, P.; Gogotsi, Y.; Rosen, J.; Barsoum, M. W. X-ray photoelectron spectroscopy of select multi-layered transition metal carbides (MXenes). Appl. Surf. Sci. **2016**, 362, 406– 417,

[37] Babak Anasori, Y. Gogotsi, 2D Metal Carbides and Nitrides (MXenes), Springer, Cham, 2019.

[38] [Thorsten Schultz, Nathan C. Frey, Chem. Mater. 2019, 31, 17, 6590–6597]

[39] [Masashi Okubo, Akira Sugahara, Satoshi Kajiyama Acc. Chem. Res. 2018, 51, 591−599]

[40] Li, J., Wang, H., & Xiao, X. (2020). Intercalation in Two-Dimensional Transition Metal Carbides and Nitrides (MXenes) toward Electrochemical Capacitor and Beyond. ENERGY & ENVIRONMENTAL MATERIALS.

[41] Li, J., Wang, H., & Xiao, X. (2020). Intercalation in Two-Dimensional Transition Metal Carbides and Nitrides (MXenes) toward Electrochemical Capacitor and Beyond. ENERGY & ENVIRONMENTAL MATERIALS

[42] Mashtalir, O., Naguib, M., Mochalin, V. et al. Intercalation and delamination of layered carbides and carbonitrides. Nat Commun **4,** 1716 (2013)

[43] Kajiyama, S., Szabova, L., Sodeyama, K., Iinuma, H., Morita, R., Gotoh, K., … Yamada, A. (2016). Sodium-Ion Intercalation Mechanism in MXene Nanosheets. ACS Nano, 10(3), 3334–3341.

[44] Sang, X., Xie, Y., Lin, M.-W., Alhabeb, M., Van Aken, K. L., Gogotsi, Y., … Unocic, R. R. (2016). Atomic Defects in Monolayer Titanium Carbide (Ti3C2Tx) MXene. ACS Nano, 10(10), 9193–9200

[45] Bandyopadhyay, A., Ghosh, D., & Pati, S. K. (2018). Effects of point defects on the magnetoelectronic structures of MXenes from first principles. Physical Chemistry Chemical Physics, 20(6), 4012–4019

[46] Zhou, T., Zhao, W., Yang, K., Yao, Q., Li, Y., Wu, B., & Liu, J. (2020). Atomic Vacancy Defect, Frenkel Defect and Transition Metals (Sc, V, Zr) Doping in Ti4N3 MXene Nanosheet: A First-Principles Investigation. Applied Sciences, 10(7)

[47] Fatheema, J., Fatima, M., Monir, N. B., Khan, A. S., & Rizwan, S. (2020). A comprehensive computational and experimental analysis of stable ferromagnetism in layered 2D Nb-doped Ti3C2 MXene. Physica E: Low-Dimensional Systems and Nanostructures, 114253.

[48] Rafiq, S., Awan, S., Zheng, R.-K., Wen, Z., Rani, M., Akinwande, D., & Rizwan, S. (2019). Novel room-temperature ferromagnetism in Gd-doped 2-dimensional Ti3C2Tx MXene semiconductor for spintronics. Journal of Magnetism and Magnetic Materials, 165954.

[49] Fatima, M., Fatheema, J., Monir, N. B., Siddique, A. H., Khan, B., Islam, A., … Rizwan, S. (2020). Nb-Doped MXene With Enhanced Energy Storage Capacity and Stability. Frontiers in Chemistry, 8.

[50] Ouisse, T., & Barsoum, M. W. (2017). Magnetotransport in the MAX phases and their 2D derivatives: MXenes. Materials Research Letters, 5(6), 365–378.

[51] Hong, W., Wyatt, B. C., Nemani, S. K., & Anasori, B. (2020). Double transition-metal MXenes: Atomistic design of two-dimensional carbides and nitrides. MRS Bulletin, 45(10), 850–861.

[52] Y. Zhang, F. Li, Robust half-metallic ferromagnetism in Cr3C2 MXene, J. Magn. Magn. Mater. 433 (2017) 222–226.

[53] Z. Zhang, X. Liu, J. Yu, Y. Hang, Y. Li, Y. Guo, Y. Xu, X. Sun, J. Zhou, W. Guo, Tunable electronic and magnetic properties of two-dimensional materials and their one-dimensional derivatives, 6 (2016) 324–350.

[54] G. Gao, G. Ding, J. Li, K. Yao, M. Wu, M. Qian, Monolayer MXenes: promising half-metals and spin gapless semiconductors, Nanoscale 8 (2016) 8986–8994.

[55] M. Alhabeb, K. Maleski, B. Anasori, P. Lelyukh, L. Clark, S. Sin, Y. Gogotsi, Guidelines for synthesis and processing of two-dimensional titanium carbide (Ti3C2Tx MXene), Chem. Mater. 29 (2017) 7633–7644.

[56] M. Khazaei, M. Arai, T. Sasaki, C.-Y. Chung, N.S. Venkataramanan, M. Estili, Y. Sakka, Y. Kawazoe, Novel electronic and magnetic properties of two-dimensional transition metal carbides and nitrides, 23 (2013) 2185-2192

[58] Scheibe, B., Tadyszak, K., Jarek, M., Michalak, N., Kempiński, M., Lewandowski, M., … Chybczyńska, K. (2019). Study on the magnetic properties of differently functionalized multilayered Ti3C2Tx MXenes and Ti-Al-C carbides. Applied Surface Science

[59] Perdew, J. P., Burke, K., & Ernzerhof, M. (1996). Generalized Gradient Approximation Made Simple. Physical Review Letters, 77(18), 3865–3868.

[60] M. Naguib, M. Kurtoglu, V. Presser, J. Lu, J. Niu, M. Heon, L. Hultman, Y. Gogotsi, M.W. Barsoum, Adv. Mater. **23**, 4248 (2011)

[61] [ Mohammad Khazaei, Masao Arai , Taizo Sasaki , Adv. Funct. Mater. 2013, 23, 2185–2192]

[62] Khazaei, M., Arai, M., Sasaki, T., Estili, M., & Sakka, Y. (2014). Two-dimensional molybdenum carbides: potential thermoelectric materials of the MXene family. Phys. Chem. Chem. Phys., 16(17), 7841–7849

[63] Hu, J., Xu, B., Ouyang, C., Zhang, Y., & Yang, S. A. (2016). Investigations on Nb2C monolayer as promising anode material for Li or non-Li ion batteries from first-principles calculations. RSC Advances, 6(33), 27467–27474.

[64] R. Momeni Feili,M. Dadsetani, R. Nejatipour, A. Ebrahimian  Journal of Electronic Materials volume 49, pages 2502–2520 (2020)

[65] Zhu, J., Chroneos, A., Eppinger, J., & Schwingenschlögl, U. (2016). S-functionalized MXenes as electrode materials for Li-ion batteries. Applied Materials Today, 5, 19–24

[66] Xingzhu Chen, Zhouzhou Kong, Neng Li, Xiujian Zhao **Phys. Chem. Chem. Phys.**, 2016,**18**, 32937-32943

[67] Li, N., Meng, Q., Zhu, X., Li, Z., Ma, J., Huang, C., … Fan, J. (2019). Lattice constants-dependent anchoring effect of MXenes for Lithium-sulfur (Li-S) batteries: A DFT study. Nanoscale.

[68] Rutkowska-Zbik, D., Grybos, R. & Tokarz-Sobieraj, R. DFT investigation of molybdenum (oxo)carbide formation from $MoO_3$ . Struct Chem **23,** 1417–1424 (2012)

[69] Radzwan, A., Lawal, A., Shaari, A., Chiromawa, I. M., Ahams, S. T., & Ahmed, R. (2020) Computational Condensed Matter, 24, e00477.]

[70] Mehroz Iqbal ,Jameela Fatheema ,Qandeel Noor, Malika Rani Muhammad Mumtaz Materials today CHEMISTRY Volume 16, June 2020, 100271

[71] Zaheer Ud Din Babar, a Jameela Fatheema,a Nimrah Arif RSC Adv., 2020, 10, 25669

[72] [Jameela Fatheema, Saleem Ayaz Khan, Nimrah Arif, Mudassir Iqbal, Hamid Ullah 2021 Nanotechnology 32 085711

[73] Khazaei, M., Mishra, A., Venkataramanan, N. S., Singh, A. K., & Yunoki, S. (2019). Recent advances in MXenes: From fundamentals to applications. Current Opinion in Solid State and Materials Science.

[74] Din Babar, Z. U., Fatheema, J., Arif, N., Anwar, M. S., Gul, S., Iqbal, M., & Rizwan, S. (2020). Magnetic phase transition from paramagnetic in Nb2AlC-MAX to superconductivity-like diamagnetic in Nb2C-MXene: an experimental and computational analysis. RSC Advances, 10(43), 25669–25678

[75] Naguib, M., Halim, J., Lu, J., Cook, K. M., Hultman, L., Gogotsi, Y., & Barsoum, M. W. (2013). New Two-Dimensional Niobium and Vanadium Carbides as Promising Materials for Li-Ion Batteries. Journal of the American Chemical Society, 135(43), 15966–15969.

[76] H. Lin, S. Gao, C. Dai, Y. Chen and J. Shi, J. Am. Chem. Soc., 2017, **139**, 16235–16247

[77] T. Su, R. Peng, Z. D. Hood, M. Naguib, I. N. Ivanov, J. K. Keum, Z. Qin, Z. Guo and Z. Wu, ChemSusChem, 2018, **11**, 1–13

[78] I. Persson, L.-Å. Näslund, J. Halim, M. W. Barsoum, V. Darakchieva, J. Palisaitis, J. Rosen and P. O.Å. Persson, 2D Mater., 2018, **5**, 015002

[79] L. Karlsson, J. Birch, J. Halim, M. W. Barsoum and P. O. Å. Persson, Nano Lett., 2015, **15**, 4955–4960

[80] X. Sang, Y. Xie, M.-W. Lin, M. Alhabeb, K. L. Van Aken, Y. Gogotsi, P. R. C. Kent, K. Xiao, and R. R. Unocic, ACS Nano, 2016, **10**, 9193–920

[81] M. Naguib, O. Mashtalir, J. Carle, V. Presser, J. Lu, L. Hultman, Y. Gogotsi and M. W. Barsoum, ACS Nano, 2012, **6**, 1322–1331

[82] Sundus Gul; Martha I. Serna; Syedah Afsheen Zahra; Nimrah Arif; Mudassir Iqbal; Deji Akinwande; Syed Rizwan, Surfaces and Interfaces,2468-0230, Vol: 24, Page: 101,2021

[83] Zixin Yang; Lingfeng Gao; Hualong Chen; Feng Zhang; Optics & Laser Technology, Vol: 142, Page: 107199, 2021, 0030-3992

[84] Din Babar, Z. U., Fatheema, J., Arif, N., Anwar, M. S., Gul, S., Iqbal, M., & Rizwan, S. (2020). Magnetic phase transition from paramagnetic in Nb2AlC-MAX to superconductivity-like diamagnetic in Nb2C-MXene: an experimental and computational analysis. RSC Advances, 10(43), 25669–25678.

[85] Xin, Y., & Yu, Y.-X. (2017). Possibility of bare and functionalized niobium carbide MXenes for electrode materials of supercapacitors and field emitters.

[86] Lingfeng Gao, Chunyang Ma, Songrui Wei, Artem V. Kuklin, Han Zhang, and Hans Ågren ACS Nano **2021** 15 (1), 954-965

[87] Zaheer Ud Din Babar[1], M S Anwar, Muhammad Mumtaz, Mudassir Iqbal 2020 2D Mater. 7 035012

[88] Mogal, S. I., Mishra, M., Gandhi, V. G., & Tayade, R. J. (2012).  734, 364–378.

[89] E. Schrödinger, Physical Review **28**, 1049 (1926)

[90] M. Born, R. Oppenheimer, Annalen der Physik **389**, 457 (1927)

[91] Density Functional Theory and the Family of (L)APW-methods: a step-by-step introduction Stefaan Cottenier August 7, 2013

[92] W. Kohn, L.J. Sham, Physical Review **140**, A1133 (1965)

[93] R. Beig, B.-G. Englert, U. Frisch, P. Hänggi, K. Hepp, W. Hillebrandt, D. Imboden, R.L. Jaffe, R. Lipowsky, H. v. Löhneysen, I. Ojima, D. Sornette, S. Theisen, W. Weise, J. Wess, J. Zittartz, C. Fiolhais, F. Nogueira, M.A.L. Marques, A Primer in Density Functional Theory (Springer Berlin Heidelberg, Berlin, Heidelberg, 2003)

[94] Anisimov, Zaanen, Andersen, Physical review. B, Condensed matter **44**, 943 (1991)

[95] P. Blaha, K. Schwarz, G.K.H. Madsen, D. Kvasnicka, J. Luitz, An augmented plane wave+ local orbitals program for calculating crystal properties

[96] P. Blaha, K. Schwarz, J. Luitz, Karlheinz Schwarz, Techn. Universitat Wien, Austria (1999)

[97] Schwarz, K., Blaha, P., & Madsen, G. K. H. (2002). Electronic structure calculations of solids using the WIEN2k package for material sciences. Computer Physics Communications, 147(1-2), 71–76.

[98] Schwarz, K. (2003). DFT calculations of solids with LAPW and WIEN2k. Journal of Solid-State Chemistry, 176(2), 319–328.

[99] D.J. Singh, Plane waves, peudopotential and the LAPW method. Boston, Dortrecht (London: Kluwer Academic Publishers, 1994

[100] N. Elyashar, D.D. Koelling, Physical Review B **13**, 5362 (1976)

[101] O.K. Andersen, Physical Review B **12**, 3060 (1975)

[102] D.D. Koelling, G.O. Arbman, Journal of Physics F: Metal Physics **5**, 2041 (1975)

[103] Hamann, Physical review letters **42**, 662 (1979)

[104] E. Wimmer, H. Krakauer, M. Weinert, A.J. Freeman, Physical Review B **24**, 864 (1981)

[105] Schwarz, K. (2003). DFT calculations of solids with LAPW and WIEN2k. Journal of Solid State Chemistry, 176(2), 319–328.

[106] Vijayaprasath, G., Murugan, R., Palanisamy, S., Prabhu, N. M., Mahalingam, T., Hayakawa, Y., & Ravi, G. (2016). Role of nickel doping on structural, optical, magnetic properties and antibacterial activity of ZnO nanoparticles. Materials Research Bulletin, 76, 48–61

[107] Göde, F., & Ünlü, S. (2018). Nickel doping effect on the structural and optical properties of indium sulfide thin films by SILAR. Open Chemistry, 16(1), 757–762.